Fall 11-2018

Application of a Light Switchable System in Redirecting Escherichia coli Metabolic Fluxes

Xintong Xia

Application of a Light Switchable System in Redirecting *Escherichia coli* Metabolic Fluxes

A Thesis

Submitted to the Faculty

of

Rose-Hulman Institute of Technology

by

Xintong Xia

In Partial Fulfillment of the Requirements for the Degree

of

Master of Science in Chemical Engineering

November 2018

ROSE-HULMAN INSTITUTE OF TECHNOLOGY

Final Examination Report

Xintong Xia — Name

Chemical Engineering — Graduate Major

Thesis Title: Application of a Light-Switchable System in Redirecting Eschericia coli Metabolic Fluxes

DATE OF EXAM: April 27, 2018

EXAMINATION COMMITTEE:

	Thesis Advisory Committee	Department
Thesis Advisor:	Irene Reizman	CHE
	David Goulet	MA
	J. Peter Coppinger	BBE

PASSED X **FAILED**

ABSTRACT

Xia Xintong

M. S. Ch. E.

Rose-Hulman Institute of Technology

November 2018

Application of a Light-Switchable System in Redirecting *Escherichia coli* Metabolic Fluxes

Thesis Advisor: Dr. Irene Reizman

Optogenetics has gained increasing attention for enabling reversible and non-invasive control in biochemical engineering. The purpose of this project is to investigate the application of a genetically engineered light-switchable system, Cph8-OmpR, for controlling the accumulation of the useful central metabolite glucose-6-phosphate (G6P) in *Escherichia coli*. This could be accomplished by linking expression of an adaptor protein, SspB, which increases enzyme phosphofructokinase (Pfk) degradation, with different light intensities. Pfk is the enzyme that catalyzes the conversion of fructose-6-phosphate (F6P), an isomer of G6P from an equilibrium reaction, to fructose 1,6-biphosphate for downstream metabolism. This step is considered the major control point of G6P accumulation in the experimental bacterial strain. A mathematical model was successfully established for this system and predicted that lower red-light exposure would result in higher intracellular G6P concentration. A construct for experimental tests was successfully made, but more work on plasmid construction and strain modification is required for future experiments.

Keywords: Chemical Engineering, Optogenetics, Biomathematical Modeling

ACKNOWLEDGEMENTS

I would like to thank my thesis advisor for all the effort spent on reviewing, problem-solving and providing inspirational yet crucial suggestions about this research. I would also like to thank the members of my advisory committee for all their work and commitment to this research. Additionally, I would like to thank fellow students William McClure and his group members for their support in part of the Matlab coding. I would also like to thank fellow student Haoxiang Song for his work in supporting with building the Light Tube Array construct. I would like to thank Lab Technician Frank Cunning and Shannon Tieken for their technical support.

TABLE OF CONTENTS

Contents

LIST OF FIGURES

Figure Page

LIST OF TABLES

Tables Page

LIST OF ABBREVIATIONS

aTc	Anhydrotetracycline
CPEC	Circular polymerase extension cloning
F6P	Fructose-6-phosphate
FBP	Fructose-1,6-biphosphate
G6P	Glucose-6-phosphate
G6PDH	Glucose-6-phosphate dehydrogenase
GFP	Green fluorescent protein
LB	Luria-Bertani
LTA	Light Tube Array
OD	Optical density
PBS	Phosphate-buffered saline
PCB	Phycocyanobilin
PCR	Polymerase chain reaction
Pfk	Phosphofructokinase
Pgi	Phosphoglucose isomerase
PPP	Pentose phosphate pathway
PWM	Pulse width modulation
sfGFP	Super-folder GFP

LIST OF SYMBOLS

English symbols

D	Duty cycle
E	Enzyme
P	LED bulb power
P	Product
S	Substrate
x	Arduino input number
X	Enzyme-substrate complex

Greek Symbols

τ_{delay}	Delay time
μ	Specific growth rate parameter
ν	Stoichiometric coefficient of the reaction

Mathematical Symbols

p(t)	Production rate of sfGFP
C_i	Concentration of metabolite i
g_0	Initial sfGFP concentration
I_r	Red-light intensity
k_g	Dilution rate constant
K_M	Concentration of substrate when the reaction reaches half of its maximum
$K_{m,app}$	Apparent K_M
k_p	Production rate parameter
p_0	Initial production rate
$v_{max,app}$	Apparent v_{max}

v_{max}	Maximum rate of reaction
a, b, n	Fitting parameters
c	Setpoint
g(t)	sfGFP concentration
r	Rate of metabolic reaction
S	Substrate concentration
v	Reaction velocity

1. INTRODUCTION

With the rapid development of genetic engineering technologies, more and more complex genetic systems have been constructed, requiring precise control. Normally gene expression in such systems is controlled by chemical inducers, oftentimes sugars, antibiotics or signal molecules [1]. Although chemical inducers are often very powerful, limitations do exist as those molecules interact with extracellular environment and alter media composition [1]. With that, many researchers have discovered new systems that can be controlled by light. Reversibility is the biggest advantage of using photons rather than traditional chemical inducers. Being able to switch between two statuses without recycling the expensive effectors can significantly reduce the cost of production as it can be difficult to retrieve an inducer such as anhydrotetracycline (aTc) from the media once it is added. Additionally, gene expression can be controlled in various manners with light as its intensity, wavelength, and duration can be easily changed.

One concept of designing light-responsive systems utilizes photo-protecting groups. Essentially, the target small molecule, oligonucleotide or protein is modified with the photo-protecting group, hence staying inactive in those cages [2]. Upon irradiation, light cleaves photo-protecting groups and frees the target compound at desired location to alter gene expression [2]. On the other hand, proteins such as phytochromes from plants and cyanobacteria naturally respond to light changes. In this case, absorption of photons will cause a conformation change at the sensory protein, and then the signal will be transmitted to the connecting protein domains,

changing the function of the whole module [3]. Introducing the sensory modules Cph1 originally obtained in *Synechocystis 6803* to *Escherichia coli*, Tabor *et al.* designed a system and were able to achieve remote and reversible control of gene expression [1]. Not only did Tabor *et al.* perform several enhancements on the designed systems, they also successfully characterized the circuit dynamics with various light input signals [4]. Thus, one goal of this project was to study the system Tabor *et al.* proposed even further by observing how the system performed with a new gene of interest instead of a reporter such as green fluorescence protein.

E. coli, a widely-used organism in genetic engineering, naturally produces glucose-6-phosphate (G6P) from glucose metabolism, and this compound is processed by the enzyme phosphoglucose isomerase (Pgi) to fructose-6-phosphate (F6P) and then further metabolized by phosphofructokinase-I (Pfk-I) to fructose-1,6-bisphosphate (FBP). While G6P is essential for central metabolism, it can be used in synthesis of more valuable products such as glucaric acid [5]. By adding a degradation tag to Pfk-I, Brockman and Prather have designed a way to knock down Pfk-I expression by expressing different level of adaptor protein SspB [5]. However, the original study used aTc as the chemical inducer to control SspB expression. For this project, implementation of the light-switchable system purposed by Tabor *et al.* was investigated instead.

The last goal of this project was to summarize the two combined systems using a mathematical model. The main purpose of this model is to relate concentration changes in final product G6P, along with other important compounds in *E. coli.* central metabolism such as F6P

and proteins such as Pfk-I, to light signal input. This will provide more insights on the system and useful predictions.

2. BACKGROUND

2.1 Cph1 sensory module from cyanobacterium *Synechocystis 6803*

Phytochromes are photoreceptors that are sensitive to red or far-red light. This type of protein is essential as plants use them to determine seed germination and flowering time according to different sunlight conditions [6]. Cyanobacteria also have phytochromes to detect harmful high energy light for their escape mechanism [7]. Phytochromes consist of the chromophore phycocyanobilin (PCB) and a sensory module. It is the conformation change of the sensory module that leads to the structural change of the rest of the protein. Figure 1 below illustrates the detailed structure of the sensory module Cph1 from the cyanobacterium *Synechrocystis 6803*.

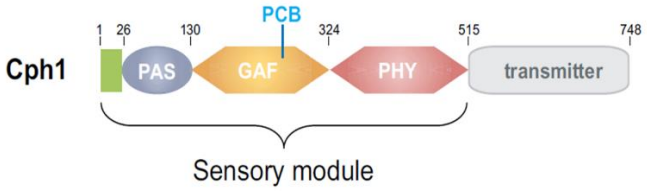

Figure 1 The simple structure of Cph1 sensory module [3].

The sensory module Cph1 contains three domains: PAS, GAF and PHY. The chromophore PCB is attached to the GAF domain and protected by part of the PHY domain from the surroundings. Upon photon activation, PCB absorbs energy and changes its structure by an isomerization reaction. This signal is then transmitted through GAF domain and enlarged by the connection between PHY and GAF domain, hence altering the structure of the whole module.

2.2 Cph8-OmpR system

EnvZ-OmpR is a natural protein-protein interaction system present in *E. coli* that regulates porin expression in response to osmotic shock. Histidine kinase EnvZ is the sensory protein while OmpR is the response regulator. Normally at high external solute concentration, EnvZ transfers a phosphate to OmpR, and phosphorylated OmpR can bind to *ompC* promoter, hence triggering gene expression [8]. To construct the light-switchable system that functions in *E. coli*, Tabor *et al.* replaced the N-terminal (extracellular and transmembrane) domain of the EnvZ protein with the sensory module Cph1 described in Section 2.1. The hybrid protein is then named Cph8, which was originally expressed individually in plasmid pCph8. In order for Cph1 sensory module to function properly, PCB is required. Therefore, Tabor *et al.* obtained genes necessary for this reaction to occur from *Synechocystis 6803* (heme oxygenase 1 and phycocyanobilin reductase) and coexpressed them in the same plasmid pPLPCB as well. The response regulator OmpR and a reporter protein sfGFP were expressed in pEO100c. With all three described plasmids expressed in *E. coli* at the same time, Tabor *et al.* were able to turn on reporter gene expression when far-red light was present and turn off gene expression when there was red light. Figure 2 is a simple illustration of how the light-switchable system functions.

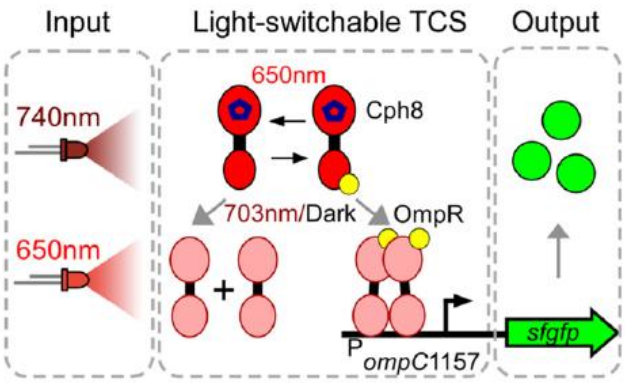

Figure 2 Cph8-OmpR light-switchable system is activated in the dark while deactivated upon exposure to 650 nm red light [1].

After several genetic modifications and rounds of screening, Tabor *et al.* finally simplified the light-switchable system into two plasmids, one containing both Cph8 and PCB production genes (pSR33.4), the other containing the reporter protein and the response regulator (pSR59.4) [1].

2.3 Manipulation of G6P levels for control of metabolic fluxes

The production of *myo*-inositol via expression of INO1 from *Saccharomyces cerevisiae* is essential for producing more useful compounds such as glucaric acid in *E. coli* [5]. Although previous studies have indicated that glucaric acid production in *E. coli* can reach 100% theoretical yield, this requires that enough G6P supply directed to this pathway by sacrificing central metabolism [5]. Thus, dynamic control of G6P level becomes important in order to balance both G6P accumulation and central metabolism. According to Brockman and Prather, this can be achieved by controlling solely Pfk-I level after a few modifications on the strain [5].

Figure 3 below illustrates these modifications [5]. Glucose-6-phosphate dehydrogenase (G6PDH) was knocked out to avoid carbon flux into the pentose phosphate pathway, as well as the isozyme Pfk-II because Pfk-I shows over 90% of phosphofructokinase activity in *E. coli* [5]. Meanwhile phosphoglucose isomerase (Pgi) was kept as the interconversion between G6P and F6P was believed to stay at equilibrium.

A chimeric version of Pfk-I with an addition of a modified SsrA tag to the enzyme was used to knock down Pfk-I level [5]. The SsrA tag can be recognized by an adaptor protein SspB, which tethers the whole substrate complex to ClpXP protease [9]. The degradation delivery complex drastically increased substrate degradation, therefore reducing F6P conversion to FBP, hence accumulating G6P.

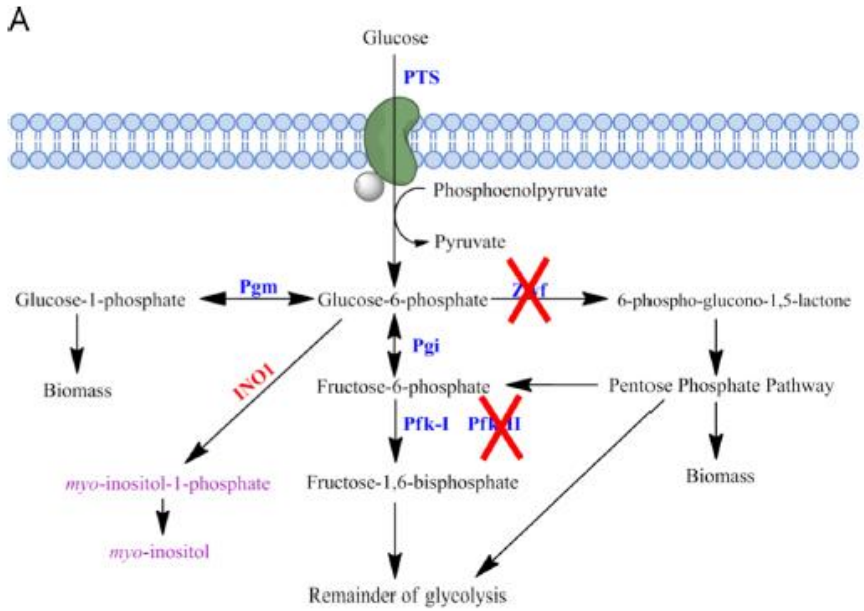

Figure 3 Zwf and Pfk-II were knocked out in *E. coli* so that Pfk-I becomes the only control point of G6P accumulation [5].

2.4 Mathematical models for optogenetic systems

Olson *et al.* had designed and built a light tube array (LTA) to study the Cph8-OmpR light-switchable system [4]. This instrument can hold many culture tubes with LED lights underneath them. By programming the LED lights, various amount of light exposure can be obtained, creating different experimental conditions. The protein of interest in their study was a reporter protein called superfolder green fluorescent protein (sfGFP) which produces fluorescence upon external activation of expression using light at certain wavelength. Therefore, flow cytometry was then used to examine the amount of fluorescence present in the culture tube after incubation. In their study, Olson *et al.* developed the following two-dimensional ordinary differential equations to describe how light input affect targeted protein concentration in Cph8-OmpR system [4].

$$\frac{\mathrm{dp(t)}}{dt} = k_p\left(c\left(t-\tau_{delay}\right)-p(t)\right) \tag{1}$$

$$\frac{\mathrm{dg(t)}}{dt} = k_g\left(p(t)-g(t)\right) \tag{2}$$

$$c(t) = \begin{cases} c_{precondition} & : \ t < \tau_{delay} \\ c(t) & : \ t \geq \tau_{delay} \end{cases} \tag{3}$$

where p(t) is the production rate of sfGFP, $\mathrm{I_r}$ is the exposed red-light intensity, $\mathrm{k_p}$ is the production rate parameter associated with red light exposure, and $\mathrm{c(t)}$ is the setpoint. The set point is what the production rate approaches in the long term, which is dependent on light intensity according to the nature of this system. Similarly, $\mathrm{g(t)}$ is the abundant sfGFP amount, $\mathrm{k_g}$ is the dilution rate constant, and $\mathrm{p_0}$ is the initial conditions. τ_{delay} is the delay time of

response to various changes in light input. Since for each test samples, there is no change in light exposure during incubation time, it is considered zero hence neglected from Equation 1. Although the original paper failed to explain the difference in units of p(t) and g(t), this project continued with this differential equation set. When t is greater than the system delay time, the set point $c(t)$ is determined by steady-state transfer function obtained from experimental data, and this relation is demonstrated in Equation 4 below [4]:

$$c(t) = b + a\frac{k^n}{(I_r^n(t)+k^n)} \tag{4}$$

where a, b, k and n are constants obtained from the repressing Hill's function fit according to experimental data. This model provides a preliminary description on how the Cph8-OmpR light-switchable system produces and accumulates the targeted product with respect to various light intensities. In the actual modeling, the targeted product is adaptor protein SspB rather than reporter protein sfGFP, but the production rate p(t) and accumulation g(t) of SspB is assumed the same as sfGFP.

In 2016, Olson et al. further improved their optogenetic model by describing the system in a different approach [21] from a microscopic point of view. Specifically, the new model is divided into a "sensing model" and an "output model" [21]. In the sensing model, both active state (S_a) and ground state (S_g) of the photoreceptors are considered [21]. Upon receiving some photon flux (n_{light}) at a particular wavelength, the sensing model produces populations of S_a and S_g with various ratios depending on the power of the light source [21]. The production rate of the

target gene (k_G), for example GFP, is related to $\frac{S_a}{S_g}$. In this model, the conversion parameters between ground state and active state can be directly calculated by measuring the photocoversion cross sections σ_g and σ_a. Figure 4 below demonstrates the new model. It is recommended to continue this project in the future with this photoconversion model since Olson et al. proved the high accuracy of this model. In addition, this approach resolves the discrepancy of the units between production rate p(t) and abundant sfGFP amount g(t) described in Equations 1 and 2.

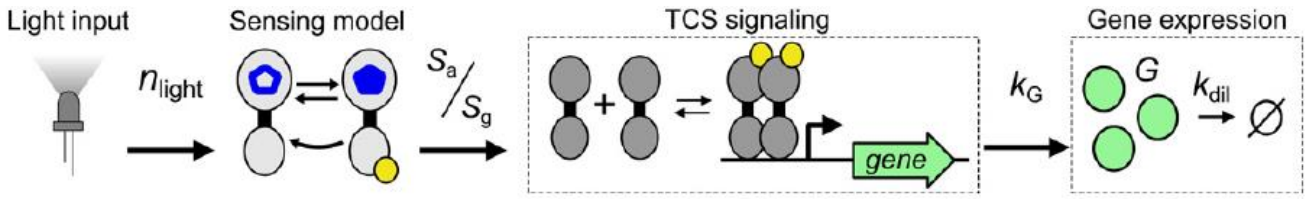

Figure 4 Schematic that describes the new optogenetic model where the target gene expression is determined from the ratio between ground-state and active-state photoreceptors.

3. METHODS

3.1 Light Tube Array (LTA) design

As the SolidWorks drawing indicates in Appendix A, the construct of the LTA is designed to accommodate 12 culture tubes. The diameter of the well is smaller than the lid of the culture tube so that tubes can be held in position. The cutout in the bottom is designed to fit two circuit breadboards, taking the height of the breadboards and electronic components into consideration. The block is made of foam, which is opaque enough to prevent external light interference from the environment as well as red light interaction among wells. There is also a foam lid (not shown in the drawing) that covers the top.

In addition, a plastic base is made by laser cut to secure the foam block on a shaking incubator (Appendix B). The holes are designed for screws to fix the whole construct on the shaker, and the distances are determined by the distribution of screw holes originally located on the incubator.

The circuit that controls the red LED lights consists of 5 transistors, 4 resistors and 4 LED light bulbs in one branch, and there are two branches. The LED light is specifically chosen to produce 640 nm wavelength red-light, which is consistent with previous studies [1,4]. According to Appendix C, the leading transistor controls the 5V input by fast PWM Mode at pin 3 or pin 11 from an Arduino UNO board. By changing the input frequency in Arduino software, various red-

light intensity levels can be obtained. Additionally, the LED lights can be turned on or off for a specified time period via programming in Arduino. An example of Arduino code is shown in Appendix D.

3.2 Light intensity measurement

To determine the corresponding red-light intensity from Arduino input number, the maximum brightness is measured by a photometer from physics department. Detailed calculation for maximum red-light intensity can be seen in Appendix E. The following equation [11] is used to calculate light intensity for a certain Arduino input number x:

$$D = \frac{x+1}{256} \times 100\% \tag{5}$$

$$P = D \times \text{maximum intensity} \tag{6}$$

where D is the duty cycle (unitless). P is the power in watts from the LED and it is assumed to be completely absorbed into the bacterial culture.

3.3 Strains and plasmids

In the beginning, MG1655 *envZ::*Kan (JW3367-3) was chosen for plasmid transformation to verify the Cph8-OmpR system. This strain can also be used to provide a template for amplification of the kanamycin cassette containing FRT sites for knocking out the *envZ* gene in other strains. However, no GFP expression was observed after transformation with plasmids pSR33.4r and pSR59.4 into JW3367-3, which was consistent with the results reported by another

group [13]. Therefore a new strain JT2 Δ*metE* Tn7::P_{cpc}G2Δ59-metE (SKA974) was used instead. The two plasmids pSR33.4r and pSR59.4 that support functionality of Cph8-OmpR system were obtained from Addgene. pSR33.4r harbors the hybrid Cph8, and it is spectinomycin resistant. pSR59.4 harbors the response regulator OmpR along with the reporter protein sfGFP, and it is ampicillin resistant. Note that the parent strain of SKA974 is RU1012, which has a parent strain MC4100. MC4100 has mutation in *rpsL*, which confers streptomycin resistance, therefore only spectinomycin can be used to retain pSR33.4r. Deletion of the native *envZ* gene in strain MG1655 Δ*endA*-zwf-pfkB-sspB pfkA::114-pfkA(DAS+4), named as IB1643 from the original study by Prather and Brockman [5], was attempted using lambda-red mediated recombination [15], yet it was not successful. Table 1 shows the strains and plasmids used in this study.

Table 1 Strains and plasmids used in this work

	Genotype	Source/citation
Strains		
JW3367-3	MG1655*Δ(araD-araB)567 ΔlacZ4787*(::rrnB-3)λ^- *ΔenvZ738::kan rph-1Δ(rhaD-rhaB)568 hsdR514*	CGSC [12]
SKA974	JT2 Δ*metE* Tn7::P_{cpc}G2Δ59-metE	Addgene
IB1643	MG1655 Δ*endA*-zwf-pfkB-sspB pfkA::114-pfkA(DAS+4)	Prather Lab [5]
Plasmids		
pSR33.4r	$Spec^R$, expresses Cph8, ho1 and PcyA constitutively	Addgene [1]
pSR59.4	Amp^R,express OmpR constitutively from P_{ompB}97 and sfGFP under the P_{ompF}146 promoter	Addgene [1]
pKD46	*ori*R101, *rep*A101ts, Amp^R, *ara*C, araBp-λγ-λβ-λexo	CGSC [15]

To construct the new reporter protein to control SspB expression, the SspB fragment was

amplified from IB1643 with 25 bp anneal region attached to the primers, which provides plasmid overlap for cloning into pSR59.4. To replace the sfGFP sequence present in pSR59.4 with sspB, circular polymerase extension cloning [16] was conducted, but this attempt was not successful. More information on the unsuccessful attempts will be discussed in the Results section with justifications, and the promising solutions will be provided in Conclusion and Future Work section.

Colony PCR with OneTaq master mix was used to screen for correct colonies along the process. Amplified PCR product for cloning was obtained using Q5 polymerase. Enzymes used in PCR and restriction digests were purchased from New England Biolabs. The primers used in this work are presented in Table 2 below:

Table 2 Primers used in this work

	Sequence	Usage
XX1	CAATCACGAACAGGCAGAGC	Check the presence of SspB in IB1643
XX2	GCATCGAAAAAGACTGGTACACGC	Check the presence of SspB in IB1643
XX3	CTCCCGCGATAAGCTGATGAACC	Amplify Kan cassette from JW3367-3
XX4	TTCTCCGGAACAGTGGCAGGAAA	Amplify Kan cassette from JW3367-3
XX5	TGAAGATCTCCAGGCATCAAATAAAAC	Linearize pSR59.4 without sfGFP
XX6	TATTTATTACCCTCATGGTTTTTTTTATGACAC	Linearize pSR59.4 without sfGFP
XX7	GTGTCATAAAAAAAACCATGAGGGTAATAAATA ATGGATTTGTCACAGCTAACACCACG	Amplify SspB with 25 bp anneal
XX8	GTTTTATTTGATGCCTGGAGATCTTCATTACTTC ACAACGCGTAATGCCG	Amplify SspB with 25 bp anneal
XX9	TAGCACTTTCACGGTAGCGA	Verify GFP absence in new plasmid
XX10	GTAGAGAGCGTTCACCGACA	Verify GFP absence in new plasmid

3.4 Culture medium and conditions

Cultures were grown in Luria-Bertani (LB) medium with appropriate antibiotics at 30℃ or 37℃ for genetic manipulation, depending on whether the plasmids used were temperature sensitive. When verifying the light-switchable system *in vivo*, LB was also used as bacteria grows faster. At the start of the experiment, 3 μL overnight culture was added to new medium. The culture tube was then placed into the LTA on a shaker at 37℃ at 250 rpm. After a specified growth time, cells were harvested by pipetting 1 mL bacterial culture into 1.7 mL microcentrifuge tubes. After centrifuging and discarding supernatant, the cell pellets were resuspended in 1X PBS solution. 200 μL samples were added to a 96-well microplate. A Spectra Gemini plate reader was used to record fluorescence at excitation wavelength of 485 nm and emission wavelength of 510 nm. Additionally, optical density (OD) at 630 nm was recorded with a BioTek plate reader and was used to normalize fluorescence readings.

3.5 Light exposure

The idea of staggered-start light induction was borrowed from the original study conducted by Olson *et al.* [4]. Each tube begins with the identical starting condition (3 μL overnight culture in 3 mL fresh media). The tubes are exposed to the same light sequence with different delay time [4]. For example, if tube A was to be treated with 3-hour red light and tube B was to be treated with 5-hour red light, tube A will receive red light 2 hours later than tube B in this 5-hour incubation. In that way, handling samples become easier, as the LTA is only installed or

removed from the shaker once per experiment.

3.6 Mathematical model development

3.6.1 Parameters used in protein degradation system

The Michaelis-Menten model is a widely used kinetics model to describe enzyme activity. It assumes the product forming reaction is rate-limiting and the complex forming reaction is equilibrated as described below:

$$E + S \rightleftharpoons ES \longrightarrow E + P$$

where E represents the enzyme, S is the substrate, P is the product and ES is the substrate complex. Writing out the differential equations and simplifying them, the famous Equation 7 can be obtained:

$$v = \frac{V_{max}[S]}{K_M + [S]} \tag{7}$$

where v is the reaction velocity, V_{max} is the maximum rate of reaction, $[S]$ is the substrate concentration, and K_M is the concentration of substrate when the reaction reaches half of its

maximum.

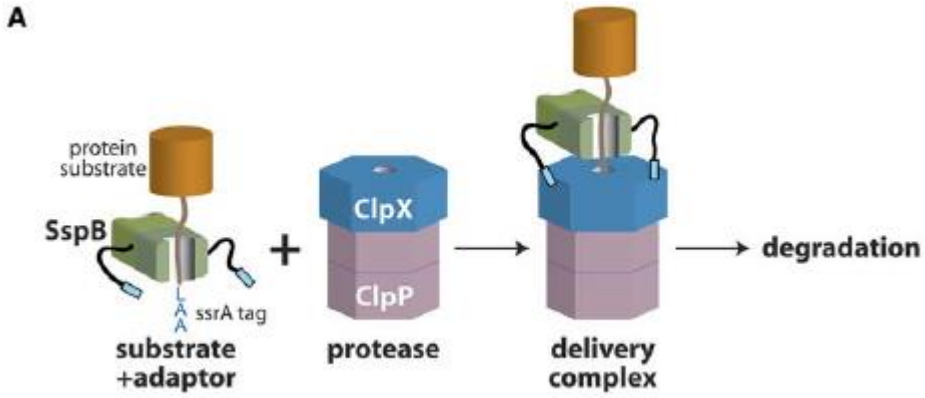

Figure 5 Diagram showing protein degradation via recognition of SsrA-tag from adaptor protein SspB [9]

As Figure 5 illustrates, the ClpXP degradation system also follows similar mechanics:

$$E_1 + S \rightleftharpoons X_1$$

$$X_1 + E_2 \rightleftharpoons X_2$$

$$X_2 \rightarrow E_2 + E_1 + P$$

where E_1 is SspB protein, S is the SsrA-tagged substrate, and E_2 is the ClpXP protease. Upon the first reaction, the SspB adaptor tethers the substrate to form a complex X_1, then X_1 reacts with the protease to form a new complex X_2. X_2 is the delivery complex which results in degradation of S and returns E_1, E_2 and degraded substrate P. Assuming the concentration of both complexes X_2 and X_1 rapidly reaches steady-state, and the product formation step is rate-limiting, the process was modeled using Michaelis-Menten kinetics. This is only an initial start to model this degradation system based on intuitive knowledge, regardless of the details listed in the reactions above. Equation 8 shows the basic form of degradation where the enzyme Pfk-I is the SsrA-tagged substrate.

$$degradation = \frac{\mathrm{V}_{max}[pfk]}{K_{m,app}+[pfk]} \quad (8)$$

The constant $\mathrm{K}_{m,app}$ can be estimated according to experimental data from existing studies [9]. Since the concentration of adaptor protein SspB is a variable, the maximum velocity v_{max} becomes a function of SspB concentration rather than a constant. It is assumed that the relationship between v_{max} and SspB also follows Michaelis-Menten kinetics. The new degradation term is described below in Equation 9:

$$\mathrm{degradation} = \frac{\mathrm{v}_{max,app}\left(\frac{[sspB]}{K_{m,sspB}+[sspB]}\right)[pfk]}{K_{m,app}+[pfk]} \quad (9)$$

where $\mathrm{K}_{m,sspB}$ is assumed to be the association constant between the substrate and adaptor protein from the original study [9] and $\mathrm{v}_{max,app}$ is estimated from the experimental data. Appendix F shows the detailed derivation for modeling this degradation system.

A more proper form is derived in Appendix P with the assumption that the concentration of the protein-protease complex remains at steady-state. The degradation expression derived in Appendix P contains one realistic solution based on the quadratic formula. Compared with Equation 8, the only variable in the derived degradation expression is the substrate (Pfk) concentration when SspB levels are held constant.

3.6.2 Parameters used in metabolic model

Assuming the sfGFP in the original Cph8-OmpR system is successfully replaced with the SspB protein, the degradation of Pfk-I can then be controlled by the expression level of SspB. To predict how changes in Pfk-I concentration affect associated metabolites in *E. coli*, the dynamic models which Chassagnole *et al.* developed become useful. Equation 10 below shows the basic form of the mass balance [10]:

$$\frac{dC_i}{dt} = \sum_j v_{ij}\, r_j - \mu C_i \tag{10}$$

where C_i is the concentration of metabolite, μ is the specific growth rate parameter, r is the rate of reaction and v is the stoichiometric coefficient of that reaction. The reaction rate r is determined from the actual enzyme kinetics along with any activation or inhibition effects. Often intracellular metabolites have many reactions associated with them and these reactions are sometimes connected. Appendix N shows a list of assumptions used to simplify the differential equations.

The following differential equations indicate how G6P and F6P are influenced by associated reactions in wild type *E. coli* [10].

$$\frac{dC_{g6p}}{dt} = r_{PTS} - r_{PGI} - r_{G6PDH} - r_{PGM} - \mu C_{g6p} \tag{11}$$

$$\frac{dC_{f6p}}{dt} = r_{PGI} - r_{PFK} + r_{TKb} + r_{TA} - 2r_{MurSynth} - \mu C_{f6p} \tag{12}$$

where the subscript denotes the corresponding enzymes. From the steady-state flux distribution diagram presented by Chassagnole *et al.* (Appendix G), the terms r_{PGM} and $r_{MurSynth}$ can be

ignored as these are minor consumptions. The return of F6P from the pentose phosphate pathway (PPP) was assumed to be half of the carbon flux entering the PPP [5]. Equation 15 describes the concentration change of enzyme Pfk in wild type *E. coli*, where the formation rate P_{pfk} is assumed to be a constant and Appendix H shows how this constant was estimated. According to Zhao *et al.* [19], the amount of carbon flux processed by Pgi from G6P to F6P is approximately four times of that processed by PPP. This additional information is summarized in Equation 16. The simplified Equations 13 and 14, along with Equation 15 and 16 were used to calculate the maximum velocity for each rate of reaction $v_{PTS,max}$, $v_{PGI,max}$, $v_{pfk,max}$, and $v_{G6PDH,max}$:

$$\frac{dC_{g6p}}{dt} = r_{PTS} - r_{PGI} - r_{G6PDH} - \mu C_{g6p} \tag{13}$$

$$\frac{dC_{f6p}}{dt} = r_{PGI} - r_{PFK} + 0.5r_{G6PDH} - \mu C_{f6p} \tag{14}$$

$$\frac{dC_{pfk}}{dt} = P_{pfk} - \mu C_{pfk} \tag{15}$$

$$r_{PGI} = 4r_{G6PDH} \tag{16}$$

In the experimental system, glucose-6-phosphate dehydrogenase (G6PDH) was deleted from IB1643 according to Prather and Brockman [5], therefore the flux term r_{G6PDH} as well as r_{TKb} and r_{TA} can be ignored because the carbon flux entering PPP became zero. Equation 17 describes the enzyme Pfk concentration over time in the experimental system:

$$\frac{dC_{pfk}}{dt} = P_{pfk} - \mu C_{pfk} - degradation \tag{17}$$

where the degradation term is discussed in Equation 9. It is also assumed that the maximum velocity $v_{pfk,max}$ in the experimental system changes linearly with respect to varying Pfk concentrations.

In this study, Matlab was used to numerically estimate a solution to the system of ODEs and obtain desired plots. Reconstruction of Cph8-OmpR red-light controlled gene expression model in Matlab was accomplished by fellow students McClure et al. [22]. Constants used in enzyme kinetic equations were adapted from Chassagnole *et al.* Appendix J has a list of constants and kinetic equations used in this study and Appendix K shows the Matlab code.

4. RESULTS

4.1 Verification of Cph8-OmpR system

Initially, experiments were conducted to verify that the Cph8-OmpR system functions correctly in the current laboratory settings. Normally, the presence of plasmids in the successful transformants can be verified from the phenotypes, including antibiotic resistance and desired gene expression observations (usually a reporter protein such as GFP). The presence of pSR59.4 can be verified from fluorescence observation under microscope, while the verification of the presence of pSR33.4r is not that obvious. A more direct method is to miniprep plasmids from the potentially successful transformants selected from the media containing corresponding antibiotics, run a diagnostic gel, and compare the results with positive controls (uncut plasmids).

As mentioned in the Methods section, experiments with JW3367-3 yielded no significant difference in fluorescence when compared to wild type JW3367-3 and transformants containing both pSR59.4 and pSR33.4r plasmids. This result is consistent with the result reported in a master's thesis published by Maithili Krishnan from TU Delft. According to the author, a potential reason is because JW3367-3 has much lower dynamic range of P_{ompC} compared to the JT2 based *E. coli* strain used in original testing of the plasmids [13]. Thus, strain SKA974 was used instead, as it is derived directly from strain JT2. Figure 6 shows the gel electrophresis results after miniprep of plasmids from the SKA974 transformants. pSR33.4r has 6201 bps, and pSR59.4 has 5363 bps, but the uncut plasmids are supercoiled when running on a gel. Therefore,

the two faint lines around 3kb and 4kb region in the sample column indicates the presence of the two plasmids.

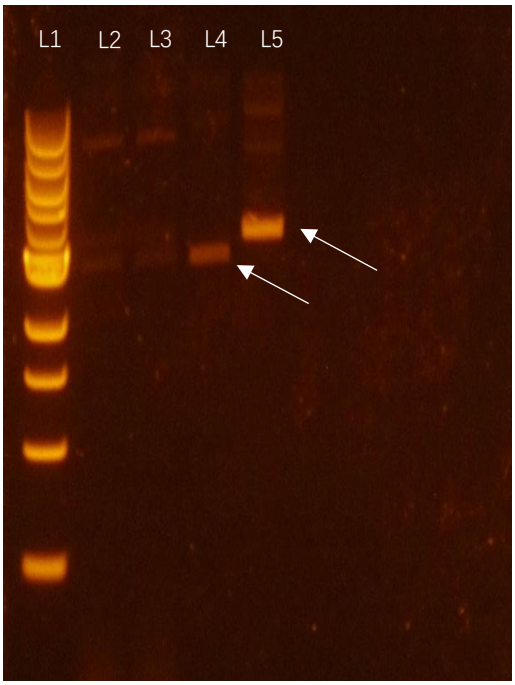

Figure 6 Gel electrophoresis of plasmid DNA indicates presence of pSR59.4 and pSR33.4r plasmids in SKA974 strain. Lane 1: 1 kb ladder; Lane 2/3: Plasmid DNA miniprepped from transformants; Lane 4: pSR59.4 DNA; Lane 5: pSR33.4r DNA.

To confirm the functionality of Cph8-OmpR system, a 21-hour run with the successful transformants was conducted. Figure 6 shows the results of fluorescence reading, indicating that the tubes incubated in dark have a higher average normalized fluorescence value than the tubes incubated under red light. At the same time, both negative controls (SKA974 strain with no plasmids), no matter exposed to red light or not, exhibit very low normalized fluorescence values. This verifies that Cph8-OmpR system functions normally in SKA974.

In addition to steady-state conditions, fluorescence values over the 21-hour run were also

tracked. Figure 7A illustrates the trend of decreasing fluorescence produced with respect to red light exposure time. Compared to the literature results presented in Figure 7B, a similar trend is observed. Thus, it appears that Cph8-OmpR system can function correctly in strain SKA974.

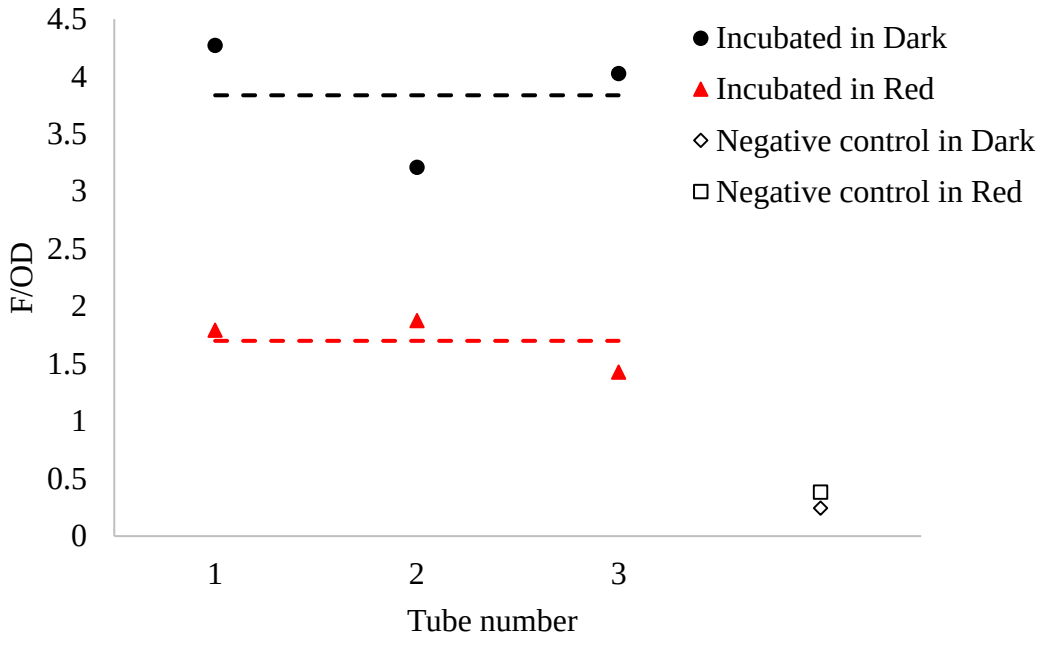

Figure 7 A higher normalized fluorescence value observed from incubation of SKA974 transformants containing both pSR33.4r and pSR59.4 plasmids in the dark compared to incubation of the same strain in the red light. Black circular dots relate to cultures incubated in dark, and red triangles relate to cultures with 21-hour red light exposure. The empty diamond indicates the negative control (plain strain with no plasmids) incubated in dark, and the empty square indicates the negative control with 21-hour red light exposure. Fluorescence readings from the plate reader are normalized against optical density reading at 630 nm. The culture was washed and resuspended in PBS before measurement on the plate reader.

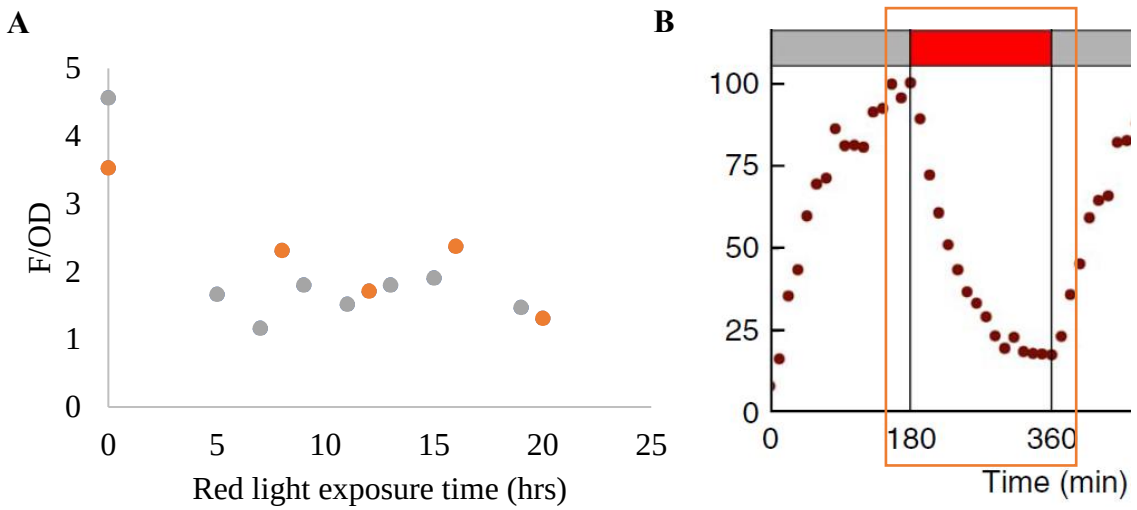

Figure 8 A) Normalized fluorescence reading of SKA974 transformants with pSR33.4r and pSR59.4 showing a descending trend with respect to time. The culture was washed and resuspended in PBS before reading. Orange dots refer to data collected on September 19th, while grey dots refer to data collected on September 20th. No replicates were taken. LED lights were set to maximum brightness in these experiments. **B) A similar trend is observed in experimental data from Olson *et al.*** where the y-axis refers to the amount of fluorescence in arbitrary units, and the x-axis refers to the time of incubation. The boxed region shows fluorescence readings under red light incubation of 1.05 W/m^2.

4.2 Attempted construction of new reporter plasmid

The protein of interest in this study is SspB rather than sfGFP, therefore a new plasmid needed to be constructed to control its expression via the Cph8-OmpR system. To accomplish this, first primers XX7 and XX8 were used to amplify SspB from wild type *E. coli*. These primers were designed to have an additional 25 bp attachments, which are the upstream and downstream homology around sfGFP in plasmid pSR59.4. The additional 25 bp homology were used in the CPEC protocol for annealing purpose. Primers XX5 and XX6 were used to linearize pSR59.4 excluding only the sfGFP region, and the resulting PCR product would be used as the plasmid backbone for SspB insertion. To check whether the insertion was successful after CPEC,

primers XX9 and XX10 were used, which would result a 674 bp fragment if SspB were inserted and an 893 bp fragment if sfGFP were still present.

While the pSR59.4 backbone without sfGFP was successfully isolated (supporting pictures are in Appendix L), no CPEC colonies showed positive results, meaning that the replacement of sfGFP with SspB was not successful. In Figure 9, the PCR product of the three sample colonies screened from an ampicillin plate did not show any band on the gel, indicating that neither SspB nor sfGFP were present at the site of amplification. One possibility was that pSR59.4 backbone had annealed to itself without adopting SspB insert. Appendix O shows the plasmid map of the desired construct.

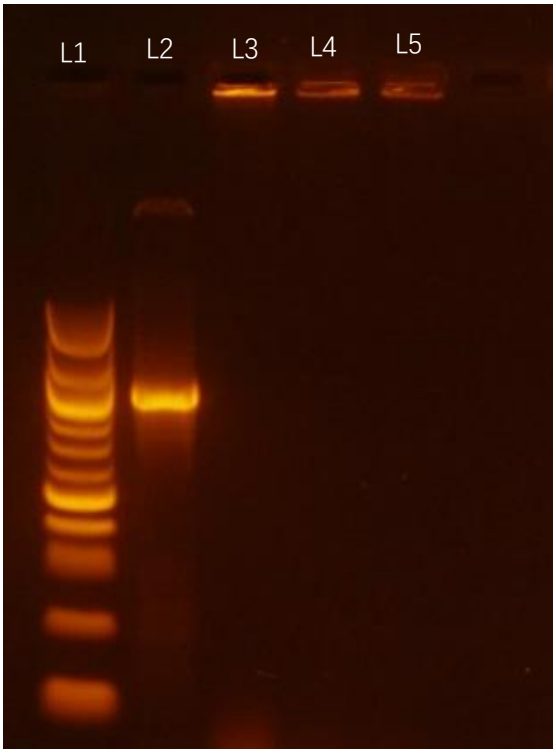

Figure 9 pSR59.4 positive control plasmid yielded a 893 bp band after colony PCR while the testing samples show no bands after PCR. Lane 1: 100 bp ladder; Lane 2: pSR59.4 positive control; Lane 3/4/5: sample CPEC colonies.

4.3 Genetic manipulation of IB1643 strain

In order for the Cph8-OmpR system to function properly, native *envZ* gene in the host strain needs to be knocked out to prevent any protein-protein interaction from inherent EnvZ-OmpR system. Lambda red recombination protocol is one approach of achieving this genetic manipulation [16]. Using strain JW3367-3, a kanamycin resistance cassette with FRT sites was amplified (Appendix K). Initially chemically competent cells were made and used after successful transformation of pKD46 plasmid. Although colonies grew on kanamycin plates, the colony PCR results indicated that native *envZ* was not successfully replaced with the kanamycin resistance cassette as shown in Figure 10. Since it was difficult to distinguish based on size of the colony PCR products (for the *envZ* fragment, the length is 1726 bp while for the kanamycin resistance cassette with FRT sites, the length is 1630 bp), restriction enzyme digest was conducted. The restriction enzyme used was EcoRI-HF, which would produce a 517 bp and 1209 bp fragments if *envZ* were present. If the replacement of *envZ* with the kanamycin resistance cassette were successful, there would be no cut using EcoRI-HF. From Figure 10, colonies 1 and 2 clearly showed two bands on the gel, as does the positive control. This indicates that these colonies still contain the *envZ* gene.

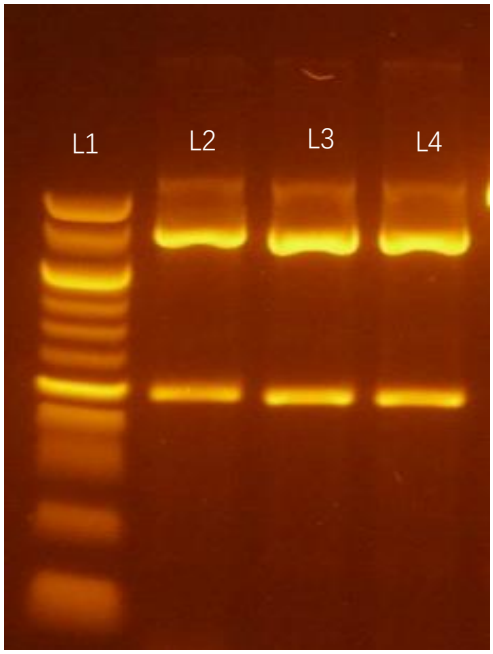

Figure 10 Experimental lambda red recombination cells show the same bands (517 bp and 1209 bp) as the positive control after colony PCR, indicating replacement of the *envZ* gene with a kanamycin resistance cassette was unsuccessful. Lane 1: 100 bp ladder; Lane 2/3: sample transformants; Lane 4: IB1643 positive control. PCR product were digested with restriction enzyme EcoRI-HF.

Chemically competent cells typically have lower transformation efficiency compared to electrocompetent cells. Therefore, the lambda red recombination protocol was also attempted with electroporation. Cells that already contained the pKD46 plasmid were first washed to eliminate all salts in the solution to prevent overheating. Then the BioRad Micropulser was used to facilitate introduction of kanamycin fragment into the washed cells. Although electroporation was believed to have higher chance of success compared to chemical transformation, no colonies were observed on the kanamycin plates.

4.4 Metabolic model

A mathematical model that connects the Cph8-OmpR system with the central metabolism of *E. coli* in strain IB1643 was built to predict important metabolite concentration changes. First, the functionality of the Cph8-OmpR system was duplicated from its original study by Olson *et al.* [4]. It was assumed that sfGFP expression controlled by light exposure could represent exactly how SspB protein expression would vary. In the simulation in Figure 11, the red light is turned on at the start of incubation and reduced to different extents at time $t = 180$ min. For I1, the light intensity changes from initially 1.05 W/m^2 to 0.0243 W/m^2; for I2, the light intensity changes from initially 1.05 W/m^2 to completely off (0 W/m^2). These values were chosen according to the original study, where I1 is the intensity value used to show a slower decline of gene expression and I2 is the maximum intensity [4]. Figure 11 illustrates that the concentration of SspB in the cell is predicted to increase when the culture is exposed to lower light intensity. This result resembles the trend described in the original study [4].

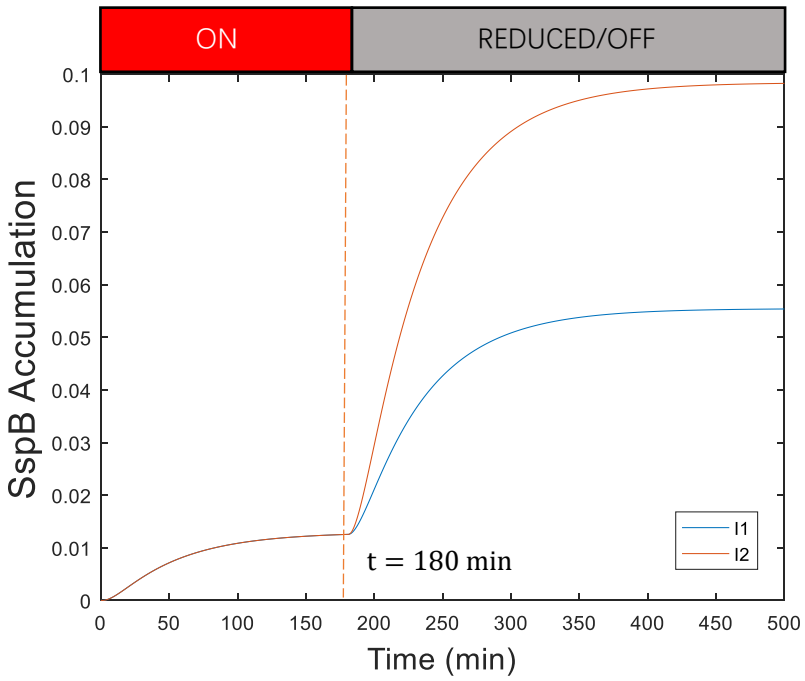

Figure 11 SspB concentration accumulates more when red light is completely off (I2) after 180 min. The concentrations are in arbitrary units.

Using the relation developed in Equation 7, a negative correlation is observed in Pfk-I concentrations at various steady-state SspB expression levels from Figure 12. The time duration in each run to generate steady-state SspB value was set to 500 min. According to the data generated in Matlab, SspB concentration quickly converged to a fixed value in a few rounds of calculation. Therefore, it is determined that the time span is sufficient for the process to reach steady-state, and the end value was used as the steady-state SspB concentration. It is obvious that more SspB can lead the SsrA-tagged Pfk-I to a protease for degradation, but this decay has a positive limit. When the system is saturated with SspB, the rate of Pfk-I degradation is approximately unchanged. Balancing between a fixed degradation rate and a constant production rate, the enzyme concentration eventually approaches an equilibrium.

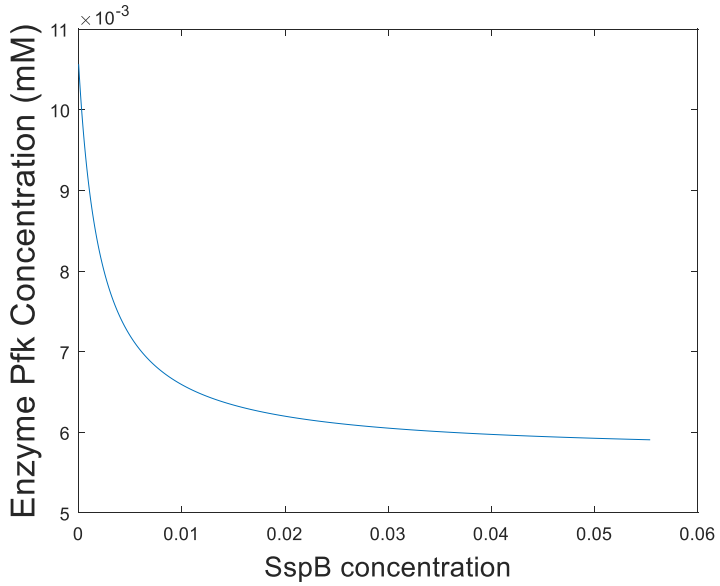

Figure 12 Pfk-I enzyme concentration decreases with increasing SspB concentration. Initial concentration estimated from steady-state enzymatic concentrations in wild type *E. coli* [17].

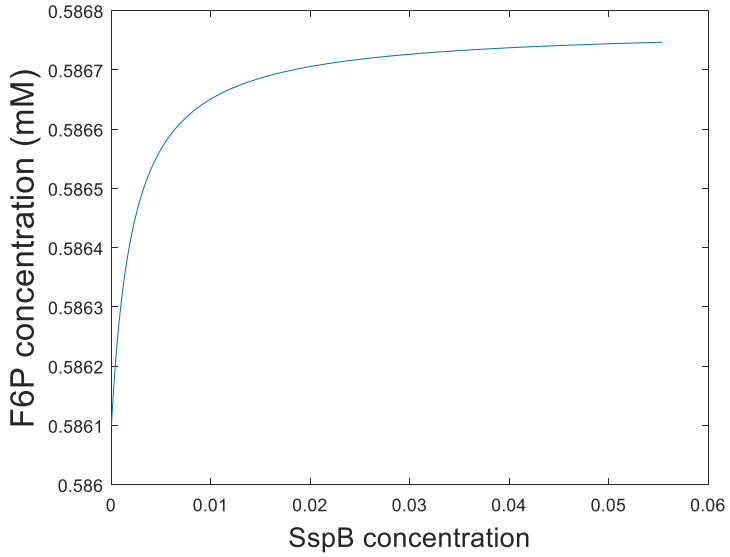

Figure 13 F6P concentration increases with increasing SspB concentration. Initial value estimated from steady-state metabolic concentrations in wild type *E. coli* [10].

Figure 13 illustrates a positive correlation between F6P and SspB concentration. A similar trend is observed in Figure 14 for G6P because it is assumed that the isomerization reaction between F6P and G6P is at equilibrium. The only difference in Figure 13 and 14 is the starting

concentrations, which are estimated from steady-state metabolite concentration in *E. coli* [10]. These two figures demonstrate how F6P and G6P concentrations vary with different SspB levels at steady-state.

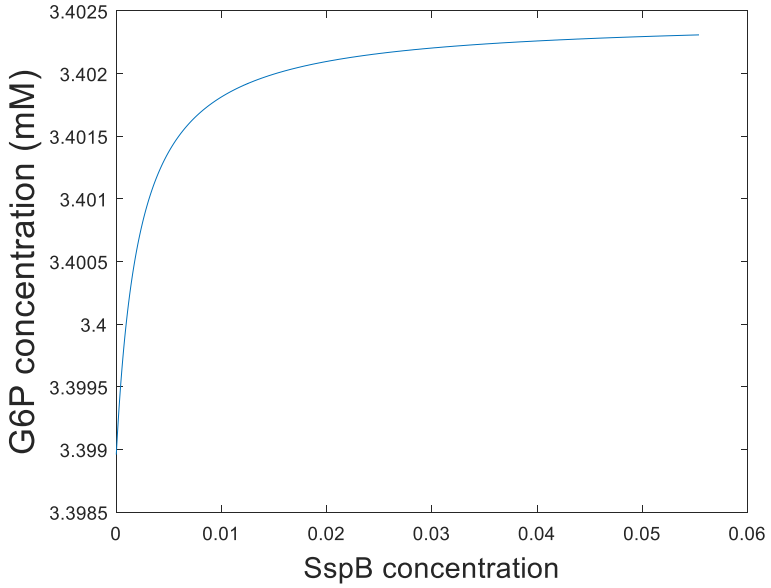

Figure 14 G6P concentration increases with respect to increasing SspB concentration. Initial value estimated from steady-state metabolic concentrations in wild type *E. coli* [10].

For a possible scenario illustrated in Figure 15, the red light is on at its maximum intensity in the beginning to inhibit SspB production. As a result, F6P would be utilized in central metabolism. After an initial growth period, red-light exposure can then be turned off or reduced, resulting an accumulation in both F6P and G6P. According to Figure 15, a reduction in red-light exposure (I1 to I2) only slightly increases intracellular G6P concentration. Considering the actual numbers, changing SspB levels only produces a little boost in G6P concentration, even with the most dramatic curve. A rough estimation on this difference of G6P is calculated in Appendix M for a 1 L pilot reactor. The resulting G6P increase from I1 to I2 is 6.19 ng. However, this number

is only based on the assumption that all the parameters used in this model are correct, which is not always true in this initial math model. Many parameters used in the model presented here come from *in vitro* values according to literature [9], while concentration of metabolites may vary inside the cell. Further work on parameter optimization is required to obtain a more accurate estimation on the improvement of G6P production.

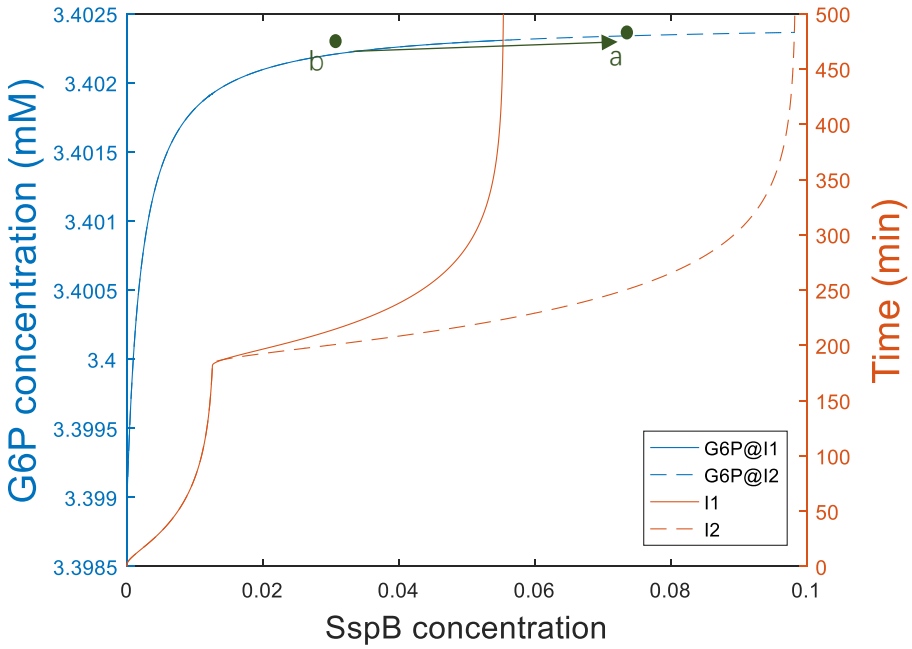

Figure 15 A practical scenario from a combined plot indicates that turning the red light completely off would produce more G6P. I1 refers to intensity change from 1.05 W/m^2 to 0.0243 W/m^2 and I2 refers to intensity change from 1.05 W/m^2 to 0 W/m^2. The blue lines (solid and dashed) follows exactly the same trend. F6P is not plotted on this figure. Following the green arrow from point b to point a, an increase in corresponding G6P can be observed.

5. DISCUSSION

Despite the many benefits of using light as an inducer or inhibitor, application of such genetic systems in real life is a challenge. Supplying oxygen to culture media is a developed process, yet dead space in the reactor is still a concern. When using light as a genetic circuit switch, normal reactors would exacerbate such problem of homogeneity because the light transmission is limited to a short range. In this case, a more delicate design such as a transparent tubular reactor is required, but it significantly reduces the convenience of regular stirred tanks. In addition, the tubular reactor should be covered with the light source to reduce environmental interference. Considering the amount of high energy generated in such a small space, heat dissipation might also become a problem. Some light-inducible systems are responsive to blue light with a short wavelength and high energy, which makes the exposure time duration particularly important. Too much blue light can be damaging to cell growth due to the large amount of energy it possesses. Finally, the cost of electricity to power the light source in production is another consideration.

The mathematical model presented in this thesis is a rudimentary prediction of the system behavior, and future works should target several areas to improve the model. First of all, the degradation model needs modifications because psuedo-steady-state analysis of the differential equations describing degradation results in a different expression than the one initially used, as described in Appendix P. The two variables in the degradation model are the Pfk concentration

and total SspB enzyme concentration, which is consistent with Equation 9. Future work should start the degradation model proposed in Appendix P with reasonable assumptions on the all the rate constants and total enzyme concentrations.

The connection between Pfk-I reduction and growth rate parameter is another factor to consider since a decrease in Pfk-I would result a slower growth. Equation 18 shows a linear relation between Pfk-I and growth rate parameter μ, which can be incorporated into future work.

$$\mu = \mu_{max} \frac{[pfk]}{[pfk]_0} \tag{18}$$

where μ_{max} is the maximum growth rate parameter, [pfk] is the Pfk-I concentration at any time, and $[\mathrm{pfk}]_0$ is the initial Pfk-I concentration.

In this study, concentration of Pfk-I was indirectly controlled by SsrA-tag and adaptor protein SspB interaction to increase the G6P pool. Alternatively, it is possible to control Pfk-I expression directly using this light-switchable system. On one hand, this method would be more direct and efficient. But on the other hand, since Pfk-I plays an essential role in central metabolism, a lot more tuning would be needed to determine the appropriate Pfk-I expression level. Although there are many parameters associated with this model, the parameter that describes Pfk-I formation has the largest impact on the behavior of the system. Sensitivity analysis could be conducted in the future to determine the influence of parameters before optimization. The rough estimation of G6P production improvement in Appendix M is insignificant, but the number could increase after proper parameter optimization.

More modifications of the circuit should be done to practically implement the Cph8-OmpR system. Currently, red lights need to be on from the beginning to the desired time point in order to promote cell growth. A more energy and cost-efficient process should have the opposite, where red lights are only turned on when they are needed. One solution is to add another layer of control besides the Cph8-OmpR system. For example, coupling a Tet-off system with the Cph8-OmpR system would reverse the circuit behavior [20]. The Cph8-OmpR would produce Tet in the dark, which turns off expression for SspB, directing all G6P for cell division. When stationary phase is achieved, the red light exposure would shut off the Cph8-OmpR system, preventing more Tet from being produced, hence turning on SspB gene expression.

6. CONCLUSION AND FUTURE WORK

In conclusion, the Cph8-OmpR system was successfully verified in this laboratory setting, as indicated by the significant difference of normalized fluorescence between two overnight incubation conditions: one completely in dark, another completely in red-light at maximum intensity. Although a similar trend was observed with declining sfGFP compared to the original study [4], it would be interesting to observe the behavior when the incubation time is less than 5 hours to confirm this. Due to time constraints for this project, implementation of the complete system with new reporter plasmid containing SspB protein was not accomplished, but the vector backbone and insert were both successfully amplified and isolated. Application of the complete system requires that the inherent *envZ* gene to be knocked out in the host strain IB1643. Several tries with chemically competent cells were not successful using the lambda red recombination protocol, and one try with electrocompetent cells resulted no colonies on selective media. Considering its higher transformation efficiency, it is recommended to perform electroporation for any future continuation of this experiment.

Using a mathematical model, it has been shown that with higher SspB expression levels, the concentrations of useful metabolites G6P and F6P also increased. The model also indicated that less red light exposure resulted in more G6P accumulation. A preliminary calculation showed that this difference is insignificant, but parameter optimization will be required to make more meaningful predictions.

As mentioned in the Discussion section, a more practical design to implement the Cph8-OmpR system is to couple it with a Tet-off system. A future direction is to experimentally combine these two systems to see whether it improves G6P accumulation or not. Using the established mathematical model as a base, the influence from Tet-off involvement as well as direct Pfk-I control can also be predicted.

The original aims of this thesis included developing a mathematical model to describe how the Cph8-OmpR red light switchable genetic system would control the production of the central metabolites G6P and F6P in *E. coli* when coupled with a SspB-controlled Pfk enzyme degradation system, and modifying the model using experimental data. For this thesis, the function of the Cph8-OmpR system was successfully verified in Rose-Hulman's laboratory settings and a light tube array was constructed for future testing. A mathematical model that links the target metabolite concentration (Pfk) with controlled input (red light) was also produced in Matlab, and the simulation showed logical trends. However, challenges were encountered when constructing reporter plasmids and gene knockouts for a new application of the Cph8-OmpR, and the tasks of parameter tuning were not finished in the given time frame.

LIST OF REFERENCES

[1] S. R. Schmidl, R. U. Sheth, A. Wu, and J. J. Tabor, "Refactoring and Optimization of Light-Switchable Escherichia coli Two-Component Systems," *ACS Synth. Biol.*, vol. 3, no. 11, pp. 820–831, Nov. 2014.

[2] L. Gardner and A. Deiters, "Light-Controlled Synthetic Gene Circuits," *Curr. Opin. Chem. Biol.*, vol. 16, no. 3–4, pp. 292–299, Aug. 2012.

[3] L.-O. Essen, J. Mailliet, and J. Hughes, "The structure of a complete phytochrome sensory module in the Pr ground state," *Proc. Natl. Acad. Sci. U. S. A.*, vol. 105, no. 38, pp. 14709–14714, Sep. 2008.

[4] E. J. Olson, L. A. Hartsough, B. P. Landry, R. Shroff, and J. J. Tabor, "Characterizing bacterial gene circuit dynamics with optically programmed gene expression signals," *Nat. Methods*, vol. 11, no. 4, pp. 449–455, Apr. 2014.

[5] I. M. Brockman and K. L. J. Prather, "Dynamic knockdown of E. coli central metabolism for redirecting fluxes of primary metabolites," *Metab. Eng.*, vol. 28, pp. 104–113, Mar. 2015.

[6] *Phytochrome*. [Online]. Available: http://plantphys.info/plant_physiology/phytochrome.shtml. [Accessed: 01-Nov-2018].

[7] R. M. W. Chau, D. Bhaya, and K. C. Huang, "Emergent Phototactic Responses of Cyanobacteria under Complex Light Regimes," *mBio*, vol. 8, no. 2, Jul. 2017.

[8] "E. coli Histidine Kinase EnvZ." [Online]. Available: http://calcium.uhnres.utoronto.ca/story/envz.html. [Accessed: 30-Mar-2018].

[9] K. E. McGinness, T. A. Baker, and R. T. Sauer, "Engineering Controllable Protein Degradation," *Mol. Cell*, vol. 22, no. 5, pp. 701–707, Jun. 2006.

[10] C. Chassagnole, N. Noisommit-Rizzi, J. W. Schmid, K. Mauch, and M. Reuss, "Dynamic modeling of the central carbon metabolism of Escherichia coli," *Biotechnol. Bioeng.*, vol. 79, no. 1, pp. 53–73, Jul. 2002.

[11] "Arduino - SecretsOfArduinoPWM." [Online]. Available: https://www.arduino.cc/en/Tutorial/SecretsOfArduinoPWM. [Accessed: 08-Mar-2018].

[12] "Strain - JW3367-3." [Online]. Available:

http://cgsc2.biology.yale.edu/Strain.php?ID=108790. [Accessed: 30-Mar-2018].

[13] M. Krishnan, "Control of gene expression in E. coli using light induction," M.S. Thesis, Life science and Technology, Delft University of Technology, 2014. Accessed on: Oct., 28, 2016 [Online]. Available: https://repository.tudelft.nl/islandora/object/uuid:c339da34-8009-4815-8bc9-32547e34227b/

[14] "Rate of translation by ribosome at 37°C as a - Bacteria Escherichia coli - BNID 100059." [Online]. Available: http://bionumbers.hms.harvard.edu/bionumber.aspx?&id=100059&ver=39. [Accessed: 14-Mar-2018].

[15] K. A. Datsenko and B. L. Wanner, "One-step inactivation of chromosomal genes in Escherichia coli K-12 using PCR products," *Proc. Natl. Acad. Sci. U. S. A.*, vol. 97, no. 12, pp. 6640–6645, Jun. 2000.

[16] J. Quan and J. Tian, "Circular Polymerase Extension Cloning of Complex Gene Libraries and Pathways," *PLOS ONE*, vol. 4, no. 7, p. e6441, Jul. 2009.

[17] P. Lu, C. Vogel, R. Wang, X. Yao, and E. M. Marcotte, "Absolute protein expression profiling estimates the relative contributions of transcriptional and translational regulation," *Nat. Biotechnol.*, vol. 25, no. 1, pp. 117–124, Jan. 2007.

[18] "sspB - Stringent starvation protein B - Escherichia coli (strain K12) - sspB gene & protein." [Online]. Available: http://www.uniprot.org/uniprot/P0AFZ3. [Accessed: 30-Mar-2018].

[19] J. Zhao, T. Baba, H. Mori, and K. Shimizu, "Effect of zwf gene knockout on the metabolism of Escherichia coli grown on glucose or acetate," *Metab. Eng.*, vol. 6, no. 2, pp. 164–174, Apr. 2004.

[20] "Tet-On/Off Technology | Solution to induce a gene on demand | genOway." [Online]. Available: https://www.genoway.com/technologies/tet/tet-system.htm. [Accessed: 14-May-2018].

[21] E. J. Olson, C. N. Tzouanas, and J. J. Tabor, "A photoconversion model for full spectral programming and multiplexing of optogenetic systems," *Molecular Systems Biology*, vol. 13, no. 4, p. 926, 2017.

[22] W. J. McClure, C. Garner, and B. Keltz, "Cph8Ompr." Course project, Rose-Hulman Institute of Technology, Terre Haute, 2017. Accessed on: April, 26th, 2017.

APPENDIX A

Drawing for the foam block that holds culture tubes. Dimensions in the drawing are in inches.

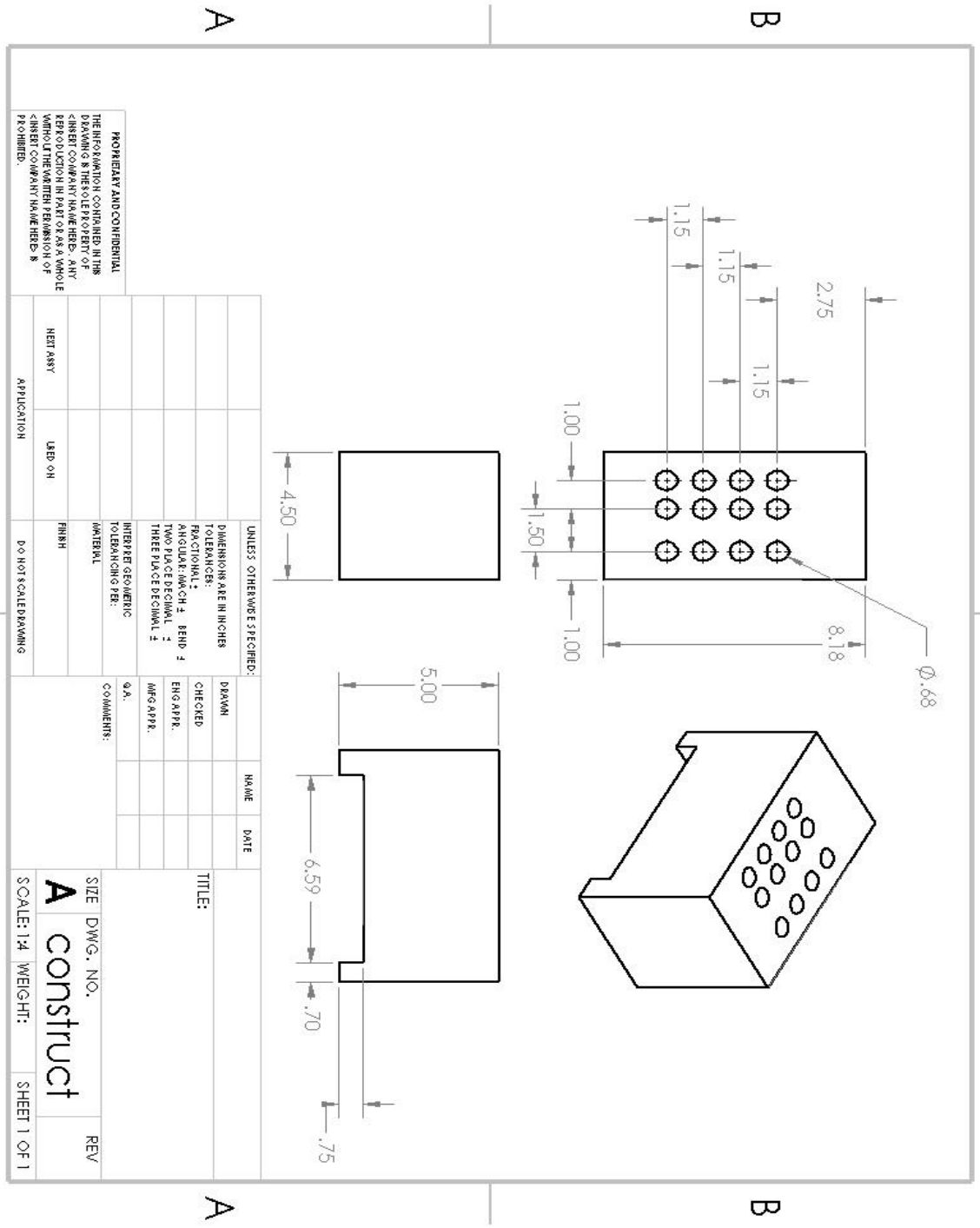

APPENDIX B

Plastic base to secure foam block on the incubator. Dimensions in the drawing are in inches.

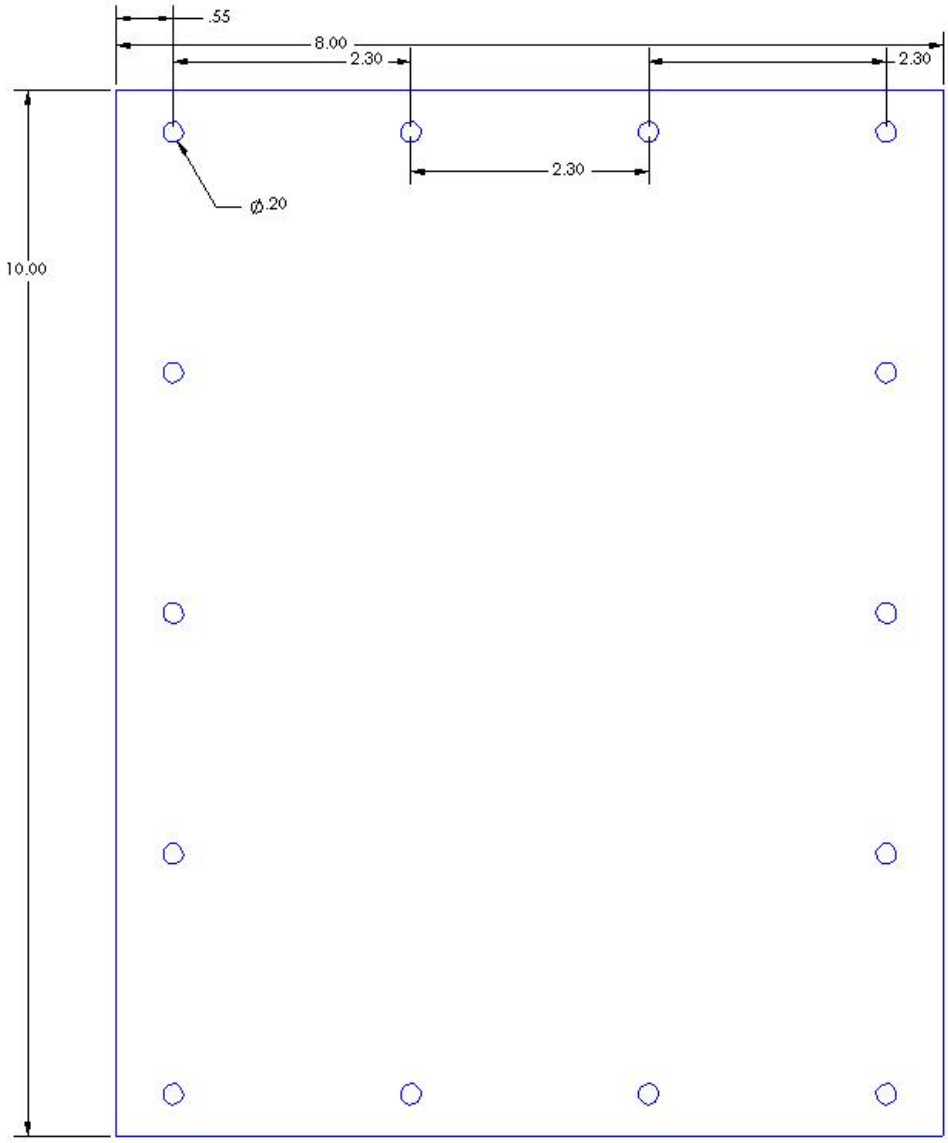

APPENDIX C

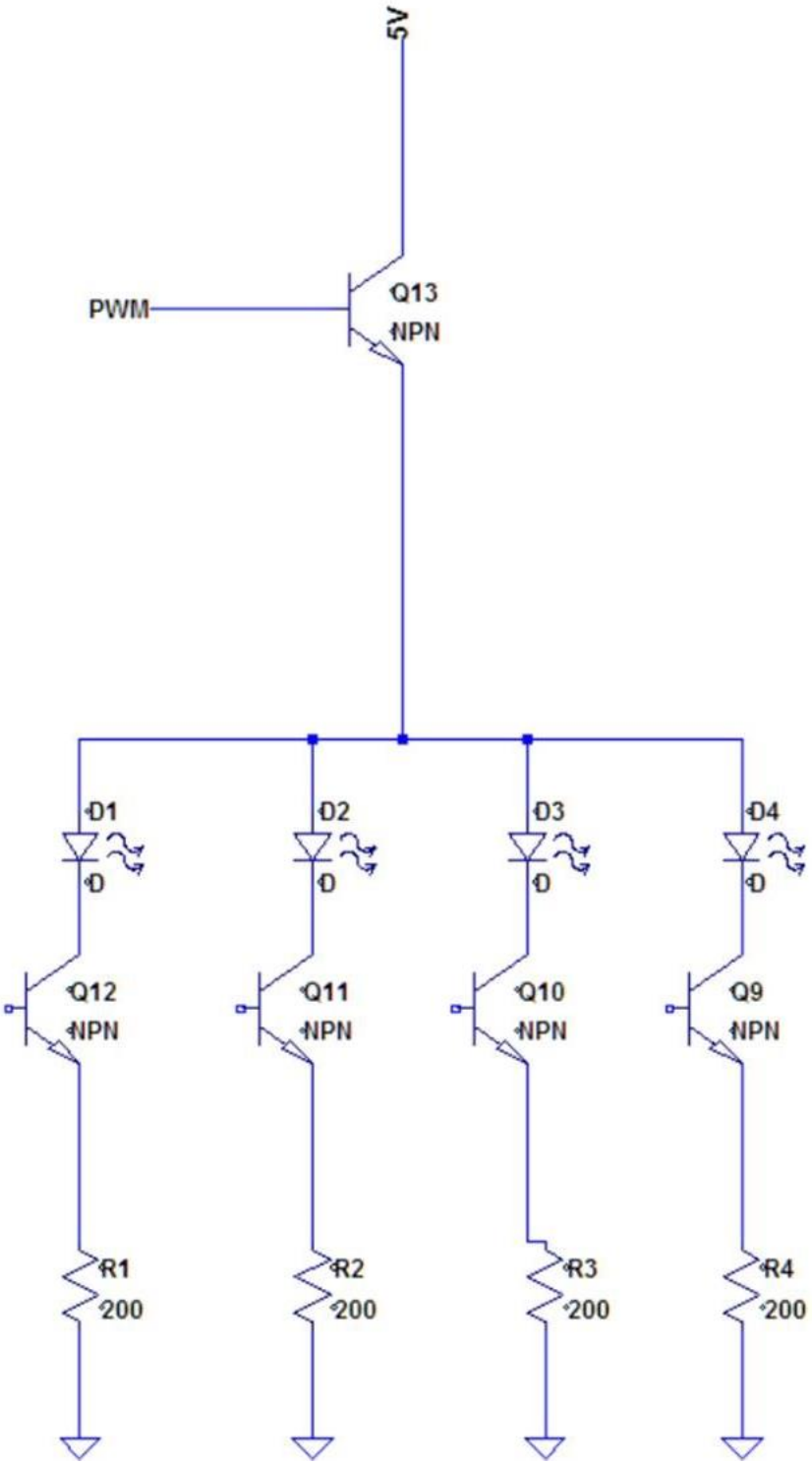
5V
PWM
Q13
NPN
D1
D
D2
D
D3
D
D4
D
Q12
NPN
Q11
NPN
Q10
NPN
Q9
NPN
R1
200
R2
200
R3
200
R4
200

APPENDIX D

Appendix D shows a sample of Arduino code used to control LED lights,

```
void setup() {
  pinMode(3, OUTPUT);
  pinMode(11, OUTPUT);
  pinMode(9,OUTPUT);
  pinMode(6,OUTPUT);
  pinMode(8,OUTPUT);
  pinMode(7,OUTPUT);
  pinMode(10,OUTPUT);
  pinMode(2,OUTPUT);
  pinMode(13,OUTPUT);
  pinMode(4,OUTPUT);

TCCR2A = _BV(COM2A1) | _BV(COM2B1) | _BV(WGM21) | _BV(WGM20);
TCCR2B = _BV(CS22);
OCR2A = 50;
OCR2B = 100;
}
void loop() {
    digitalWrite(4,HIGH);//hole 4 light on for 20 hrs for negative control
    delay(7200000);//delay 2 hours for every sample
    digitalWrite(9,HIGH); //hole 5 light on for 18 hrs
    delay(14400000);//delay 4 hours for the next light to turn on
    digitalWrite(6,HIGH);//hole 6 light on for 14 hrs
    delay(7200000);//delay 2 hrs
    digitalWrite(8,HIGH); //hole 7 light on for 12 hrs
    delay(7200000);//delay 2 hrs
    digitalWrite(7,HIGH); //hole 8 light on for 10 hrs
    delay(7200000);//delay 2 hrs
    digitalWrite(10,HIGH);//hole 1 light on for 8 hrs
    delay(7200000);//delay 2 hrs
    digitalWrite(2,HIGH);//hole 2 light on for 6 hrs
    delay(7200000);//delay 2 hrs
    digitalWrite(13,HIGH);//hole 3 light on for 4 hrs
//    delay(3000);
//    digitalWrite(4,HIGH);//hole 4
    //delay(14400000);
```

```
//   digitalWrite(9,LOW);
//   digitalWrite(6,LOW);
//   digitalWrite(8,LOW);
//   digitalWrite(10,LOW);
//   digitalWrite(13,LOW);
//   digitalWrite(7,LOW);
//   digitalWrite(4,LOW);
//   digitalWrite(2,LOW);

//   delay(600000);
}
```

APPENDIX E

Appendix E shows how light intensities were determined.
Simple schematic showing construct wells:

Hole 1 Status: ON Brightness: 432 μW	Hole 5 Status: ON Brightness: 290 μW
Hole 2 Status: ON Brightness: 323 μW	Hole 6 Status: ON Brightness: 320 μW
Hole 3 Status: OFF Brightness: 10.6 μW	Hole 7 Status: OFF Brightness: 7.5 μW

Hole 1, 2, 5, and 6 had red LED lights programmed in Arduino for maximum brightness. Using the average of the four values, an average brightness in $\mathrm{W/m^2}$ was determined (Detailed calculation are shown below). Additionally, brightness values from hole 3 and hole 7 indicate that the light interference among holes is negligible.

$$\text{Average} = \frac{432 + 290 + 323 + 320}{4} = 341.25\ \mu W$$

The sensor had a diameter of 1 cm.

$$\text{Average power per area} = \frac{341.25\ \mu\text{W} * \frac{1\ \text{W}}{10^6\ \mu W}}{\pi * \frac{(1\ cm)^2}{4} * \frac{m^2}{(100\ cm)^2}} = 4.34\frac{W}{m^2}$$

APPENDIX F

Appendix F shows how degradation model was estimated.

$$\frac{\mathrm{d[pfk]}}{dt} = P - \mu[pfk] - rate\ of\ degradation \tag{F1}$$

$$\text{rate of degardation of substrate} = \frac{\mathrm{V}_{max}[pfk]}{K_{m,app}+[pfk]} \tag{F2}$$

$$\mathrm{V}_{max} = \frac{\mathrm{V}_{max}}{[\mathrm{ClpX}_6]} * [\mathrm{ClpX}_6] \tag{F3}$$

Constants can be determined from Figure 2D from McGinness *et al.*

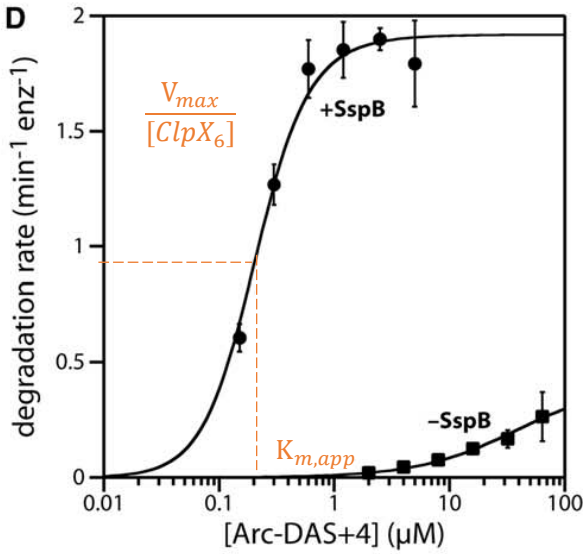

Figure F1 Experimental characterization of protein degradation system ClpXP [7]

$$\frac{\mathrm{V}_{max}}{[ClpX_6]} = 2\ \left(\frac{1}{min}\right) \qquad \mathrm{K}_{\mathrm{m,app}} = 0.2\ \mu M$$

From Methods section [7]

$$[\mathrm{ClpX}_6] = 300\ \mathrm{nM}$$

The degradation velocity is dependent on both Pfk-I and SspB concentration. If [pfk] >> Km, then the following equation holds true:

$\mathrm{v} = \mathrm{f(pfk, sspB)}$, if $\mathrm{pfk} \gg \mathrm{K}_{\mathrm{m,app}}$

$$\mathrm{V}^*_{max} = \mathrm{V}_{max} * \mathrm{f(sspB)} = \mathrm{V}_{max} * \frac{[\mathrm{sspB}]}{K_m+[sspB]} \tag{F4}$$

This K_m is how well sspB binds to substrate pfk. Use K_{AS} (association constant between SspB and substrate) as an initial estimation.

$$\mathrm{K}_{AS} = 2.2\ \mu M$$

$$\text{pfk degradation} = v^* = \frac{V^*_{max} * [\text{pfk}]}{K_{m,app} + [pfk]} = \frac{V_{max}\left(\frac{[sspB]}{Km + [sspB]}\right) * [pfk]}{K_{m,app} + [pfk]} \quad \text{(F5)}$$

APPENDIX G

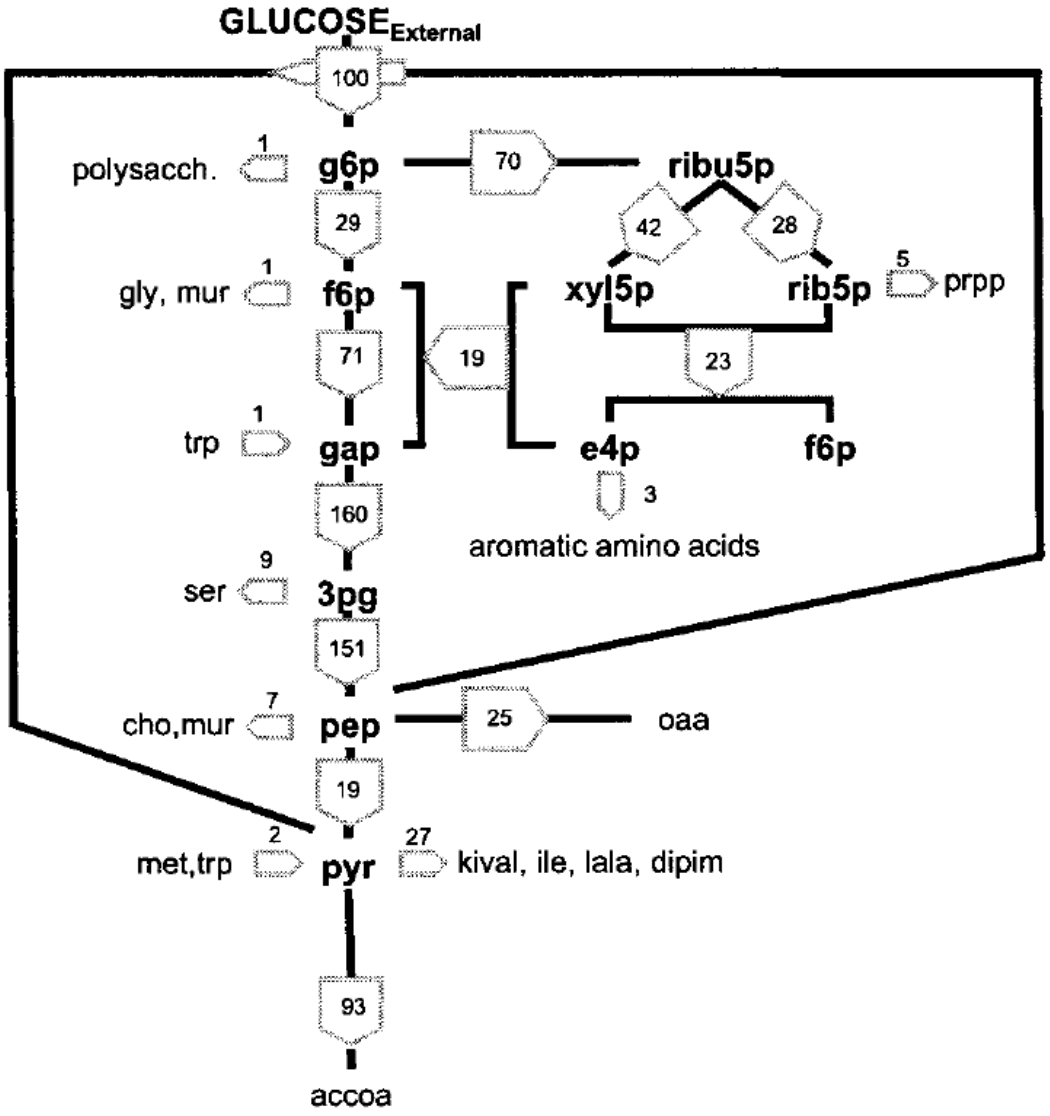

Figure G1 Flux distribution diagram from Chassagnole *et al.,* showing that the consumption of G6P by phosphoglucomutase (PGM) is minor as well as the consumption of F6P by mureine synthesis. However, the assumption that 80% carbon flux is processed through Pgi while 20% carbon is processed though PPP is contradictory to this figure. Instead, this assumption comes from authors who specifically conducted investigations on enzymes associated with G6P utilization [19].

APPENDIX H

From literature [14], the peptide chain elongation speed for *E. coli* is listed below at various growth rates at 37℃:

Table H1 Peptide chain elongation speed at different growth rate [14]

Growth rate μ [h^{-1}]	Peptide chain elongation [aa residues/s]
0.6	12
1.0	16
1.5	18
2.0	20
2.5	21

Plotting this dataset in Excel to generate a linear trend line, and this expression can be used to calculate peptide chain elongation at any growth rate. Assuming the growth rate to be 0.1 h^{-1} [10], the resulting peptide chain elongation speed is 10.96 aa/s.

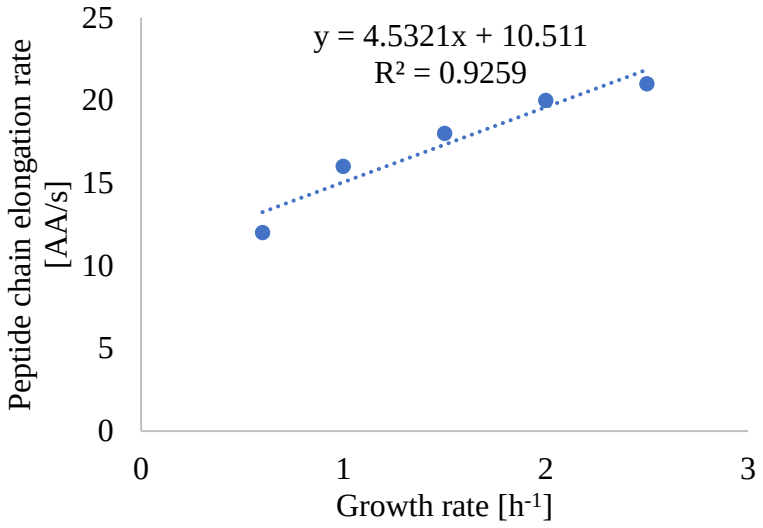

Figure H1 Linear regression of peptide chain elongation at various growth rate.

Lu *et al.* have successfully measured in vivo enzyme concentration as well as number of mRNA in *E. coli* [17]. To estimate production rate, the number of mRNA is used. The length of enzyme in number of amino acids was obtained from UniProt [18], and the volume of a single *E. coli* cell was calculated assuming it was a simple sphere with diameter of 1 μm. The information is summarized below:

Table H2 Information needed to calculate production rates

Enzyme	#mRNA [molecules/cell] [17]	AA length [aa^{-1}] [18]
PfkA	5.30117	320
SspB	3.26505	165

$$\text{production rate } \left[\frac{mM}{s}\right] = \frac{elongation\left[\frac{aa}{s}\right] * AA\ length\left[\frac{1}{aa}\right] * \#mRNA\left[\frac{molecules}{cell}\right]}{Volume\left[\frac{L}{cell}\right] * N_A\left[\frac{molecules}{mol}\right]} * 10^3 \left[\frac{mM}{M}\right] \quad \text{(H1)}$$

where N_A is the Avogadro's number.
The resulting production rate are shown below:

Table H3 Resulting production rates for the enzyme PfkA and SspB

Enzyme	Production Rate [mM/s]
SspB	$6.88 * 10^{-7}$
PfkA	$5.76 * 10^{-7}$

APPENDIX J

Appendix J shows the list of constants and kinetic equations used in the mathematical model Kinetic equations [10]:

$$r_{PTS} = \frac{v_{PTS}^{max} C_{glucose}^{extra} \frac{C_{pep}}{C_{pyr}}}{(K_{PTS,a1} + K_{PTS.a2} * \frac{C_{pep}}{C_{pyr}} + K_{PTS,a3} C_{glucose}^{extra} + C_{glucose}^{extra} * \frac{C_{pep}}{C_{pyr}}) * (1 + \frac{C_{G6P}^{n_{PTS,G6P}}}{K_{PTS,G6P}})} \quad \text{(J1)}$$

$$r_{PGI} = \frac{v_{PGI}^{max}\left(C_{G6P} - \frac{C_{F6P}}{K_{PGI,eq}}\right)}{K_{PGI,G6P}\left(1 + \frac{C_{F6P}}{K_{PGI,F6P} * \left(1 + \frac{C_{6PG}}{K_{PGI,F6P,6PGinh}}\right)} + \frac{C_{6PG}}{K_{PGI,G6P,6PGinh}}\right) + C_{G6P}} \quad \text{(J2)}$$

$$r_{PFK} = \frac{v_{PFK}^{max} C_{ATP} C_{F6P}}{\left(C_{ATP} K_{PFK,ATP,s}\left(1 + \frac{C_{ADP}}{K_{PFK,ADP,c}}\right)\right)\left(C_{F6P} + K_{PFK,F6P,s} * \frac{A}{B}\right)\left(1 + \frac{L_{PFK}}{\left(1 + C_{F6P} * \frac{B}{K_{PFK,F6P,s}^{A}}\right)^{n_{PFK}}}\right)} \quad \text{(J3)}$$

$$A = 1 + \frac{C_{pep}}{K_{PFK,pep}} + \frac{C_{ADP}}{K_{PFK,adp,b}} + \frac{C_{AMP}}{K_{PFK,AMP,b}} \quad \text{(J4)}$$

$$B = 1 + \frac{C_{ADP}}{K_{PFK,ADP,a}} + \frac{C_{AMP}}{K_{PFK,AMP,a}} \quad \text{(J5)}$$

$$r_{G6PDH} = \frac{v_{G6PDH}^{max} C_{G6P} C_{NADP}}{(C_{G6P} + K_{G6PDH,G6p})\left(1 + \frac{C_{NADPH}}{K_{G6PDH,NADPH,G6Pinh}}\right)\left(K_{G6PDH,NADP}\left(1 + \frac{C_{NADPH}}{K_{G6PDH,NADPH,NADPinh}}\right) + C_{NADP}\right)} \quad \text{(J6)}$$

Repressive Hill function equations and parameters [4]:

$$\frac{\mathrm{dp(t)}}{dt} = k_p(I_r) \times \left(c\left(t - \tau_{delay}\right) - p(t)\right) \quad (1)$$

$$\frac{\mathrm{dg(t)}}{dt} = k_g \times \left(p(t) - g(t)\right) \quad (2)$$

$$\mathrm{p}_0 = g_0 = c\left(t < \tau_{delay}\right) = c_{precondition} \quad (3)$$

$$c = b + a * \frac{k^n}{Ir^n + k^n} \quad (4)$$

Table J1 Parameters used to describe the Cph8-OmpR system

Parameters	Values
a	0.859
b	0.125
n	1.39
k	0.0243
k_g	0.0203 min^{-1}
k_p	0.177 min^{-1}
τ_{delay}	0 min
p_0	$6.88 * 10^{-7}$ mM
g_0	0 mM

Note that a and b are 1% of the fit value provided by Olson *et al.* [4]. This change was made because both a and b are in arbitrary units, and the purpose is to have a closer examination of G6P concentration change. The Hill coefficient n remains unchanged. The initial production rate of SspB p_0 is calculated in Appendix H, while the initial SspB accumulation amount g_0 is set to be zero.

Kinetic parameters [10]:

Table J2 Kinetic parameters used in rate of reaction

Enzyme	Parameters	Values
PTS	$K_{PTS,a1}$	3082.3 mM
	$K_{PTS,a2}$	0.01 mM
	$K_{PTS,a3}$	245.3
	$K_{PTS,G6P}$	2.15 mM
	$n_{PTS,G6P}$	3.66
PGI	$K_{PGI,G6P}$	2.9 mM
	$K_{PGI,F6P}$	0.266 mM
	$K_{PGI,eq}$	0.1725
	$K_{PGI,G6P,6PGinh}$	0.2 mM
	$K_{PGI,F6P,6PGinh}$	0.2 mM
PFK	$K_{PFK,f6p,s}$	0.325 mM
	$K_{PFK,ATP,s}$	0.123 mM
	$K_{PFK,ADP,a}$	128 mM
	$K_{PFK,ADP,b}$	3.89 mM
	$K_{PFK,ADP,c}$	4.14 mM
	$K_{PFK,AMP,a}$	19.1 mM
	$K_{PFK,AMP,b}$	3.2 mM
	L_{PFK}	5629067
	n_{PFK}	11.1
G6PDH	$K_{G6PDH,G6P}$	0.07 mM

	$K_{G6PDH,NADP}$	0.015 mM
	$K_{G6PDH,NADPH,NADPinh}$	0.01 mM
	$K_{G6PDH,NADPH,G5Pinh}$	0.18 mM

Growth rate [10]: $\mu = 2.78 * 10^{-5}\ s^{-1}$

Steady-state constants:

Table J3 Steady-state metabolite concentrations from Chassagnole *et al.*

Name	Concentration (mM)
$C_{glucose}^{extra}$	0.0556
C_{pep}	2.67
C_{pyr}	2.67
C_{ATP}	4.27
C_{6pg}	0.808
C_{ADP}	0.595
C_{AMP}	0.955
C_{G6P}	2.48
C_{F6P}	0.6
C_{PFK}	0.0104
C_{NADP}	0.195
C_{NADPH}	0.062

APPENDIX K

Appendix K shows the Matlab code to estimate numerical solutions to the mathematical model.

```
clc
clear variables
close all

%Steady-state concentrations from Chassagnole et al.
glu_extra = 0.0556; %mM
pep = 2.67; %mM
pyr = 2.67; %mM
atp = 4.27; %mM
pg = 0.808; %mM 6pg
adp = 0.595; %mM
amp = 0.955; %mM

pfkA=3287.39; %molecule/cell from Lu et. al
volume = 4/3*pi*(10^(-5)/2)^3; %L/cell
Na = 6.023*10^(23); %molecule/mol

pfk = pfkA/volume/Na*10^3; %mM
g = 3.48; %mM g6p
f = 0.6; %mM f6p
nadp = 0.195; %mM
nadph = 0.062; %mM

c = [glu_extra;pep;pyr;atp;pg;adp;amp;g;f;pfk;nadp;nadph]; %pg is 6pg

%Growth rate from Chassagnole et al.
mu = 2.78E-5;%(1/s)

%K value for enzyme kinetics from Chassagnole et al.
kpts_a1 = 3082.3; %mM
kpts_a2 = 0.01; %mM
kpts_a3 = 245.3;
kpts_g6p = 2.15; %mM
kpgi_g6p = 2.9; %mM
kpgi_f6p = 0.266; %mM
kpgi_f6p_inh = 0.2; %mM
kpgi_g6p_inh = 0.2; %mM
```

```
kpfk_atp_s = 0.123; %mM
kpfk_adp_c = 4.14; %mM
kpfk_f6p_s = 0.325; %mM
kpfk_pep = 3.26; %mM
kpfk_adp_b = 3.89; %mM
kpfk_amp_b = 3.2; %mM
kpfk_adp_a = 128; %mM
kpfk_amp_a = 19.1; %mM
kpgi_eq = 0.1725;
kzwf_g6p = 14.4; %mM
kzwf_nadph_ginh = 6.43; %mM
kzwf_nadp = 0.0246; %mM
kzwf_nadph_ninh = 0.01; %mM


k = [kpts_a1;kpts_a2;kpts_a3;kpts_g6p;kpgi_g6p;kpgi_f6p;...
    kpgi_f6p_inh;kpgi_g6p_inh;kpfk_atp_s;kpfk_adp_c;...
    kpfk_f6p_s;kpfk_pep;kpfk_adp_b;kpfk_amp_b;kpfk_adp_a;...
    kpfk_amp_a;kpgi_eq;kzwf_g6p;kzwf_nadph_ginh;...
    kzwf_nadp;kzwf_nadph_ninh];

% Initial Vmax set arbitrarily
vmax0=[1;1;1;1]; %rpts(max);rpgi(max);rpfk(max);rzwf(max)
% Calculate Vmax
option = odeset('NonNegative',3);
[vmax,fval] = fsolve(@(vmax)max1(c,k,vmax,mu),vmax0,option)

%Initial condition of metabolites g6p, f6p and enzyme pfk
y0 = [c(8);c(9);pfk]; %steady-state concentrations
tspan = [0 500]; %min

kg = 0.0203; kp = 0.177 %1/min from Olson et al.

%Get initial values
% twodgel= 2237.30; %molecule/cell
% sspB_int = twodgel/volume/Na*10^3; %mM
u0 = [6.88E-7, 0]; %mM vector u0 = [p0, g0], where p0 is the initial
production
                %rate of sspB and g0 is initial accumulation(zero)

%Red light intensity
```

```
%Initially on at 1.05 W/m^2
%Ir turns down from 1.05 W/m^2 to 0.0243 W/m^2
%Ir1 turns off from 1.05 W/m^2 to 0 W/m^2
Ir = @(t)1.05+(0)*(t>0)+ (-1.05+0.0243)*(t>180);
Ir1 = @(t)1.05+(0)*(t>0)+(-1.05)*(t>180);

%Define SspB concentrations at different light intensities (Ir and Ir1) at
%various time
option1 = odeset('Maxstep',1);
option2 = odeset('Maxstep',1);
[t,u] = ode45( @(t,u) Cph8Ompr_ODEs(Ir,t,u,kp,kg), tspan, u0,option1);
sspB = u(:,end);
[t,u] = ode45( @(t,u) Cph8Ompr_ODEs(Ir1,t,u,kp,kg), tspan, u0,option1);
sspB1 = u(:,end);

%Calculate the steady-state metabolite/enzyme concentrations using every
%SspB value defined above with the loop
%Steady-state is defined as the end values calculated by ode45 fucntion. The
"end values" are taking late enough in this process as the values becomes
steady very quickly in every round of calculation.

m=1;
for i=1:length(sspB)
    [t,y] = ode45(@(t,y)diffsystem(y,c,k,vmax,mu,sspB(i)),tspan,y0,option2);
   Y(m,:)=([y(length(y),1),y(length(y),2),y(length(y),3)]);
   m=m+1;
end

%Same loop function but with SspB values corresponding to Ir1 light
%intensity
p=1;
for i=1:length(sspB1)
    [t,y] = ode45(@(t,y)diffsystem(y,c,k,vmax,mu,sspB1(i)),tspan,y0,option2);
   P(p,:)=([y(length(y),1),y(length(y),2),y(length(y),3)]);
   p=p+1;
end

%Plot figures
figure
plot(sspB,Y(:,3))
xlabel('SspB concentration','Fontsize',15)
```

```
ylabel('Enzyme Pfk Concentration (mM)','Fontsize',18)
figure
plot(sspB,Y(:,1))
xlabel('SspB concentration','Fontsize',15)
ylabel('G6P concentration (mM)','Fontsize',18)
figure
plot(sspB,Y(:,2))
xlabel('SspB concentration','Fontsize',15)
ylabel('F6P concentration (mM)','Fontsize',18)
figure
plot(t,sspB(1:length(t)));
hold on
plot(t,sspB1(1:length(t)));
xlabel('Time (min)','Fontsize',15)
ylabel('SspB Accumulation','Fontsize',18)
legend({'I1','I2'})
figure
yyaxis left
plot(sspB,Y(:,1))
xlabel('SspB concentration','Fontsize',15)
ylabel('G6P concentration (mM)','Fontsize',18)
hold on
plot(sspB1,P(:,1))
yyaxis right
plot(sspB(1:length(t)),t)
ylabel('Time (min)','Fontsize',18)
hold on
plot(sspB1(1:length(t)),t)
hold on
legend({'G6P@I1','G6P@I2','I1','I2'})
axis auto


function dy = diffsystem(y,c,k,vmax,mu,sspB)
%Parameters from Chassagnole et al.
Lpfk = 5629067;
npfk = 11.1;
npts = 3.66;

%Rate of reactions
rpts =
```

```
vmax(1)*c(1)*c(2)/c(3)/((k(1)+k(2)*c(2)/c(3)+k(3)*c(1)+c(1)*c(2)/c(3))*(1+(y(
1))^npts/k(4)));

rpgi = vmax(2)*(y(1)-
y(2)/k(17))/(k(5)*(1+y(2)/(k(6)*(1+c(5)/k(7)))+c(5)/k(8))+y(1));

A = 1+c(2)/k(12)+c(6)/k(13)+c(7)/k(14);
B = 1+c(6)/k(15)+c(7)/k(16);

rpfk =
vmax(3)*y(3)/c(10)*c(4)*y(2)/((c(4)+k(9)*(1+c(6)/k(10)))*(y(2)+k(11)*A/B)*(1+
Lpfk/((1+y(2)*B/((k(11))^A))^npfk)));

%Parameters from McGinness et al.
Km = 0.2E-3; %mM
Kas = 2.2E-3; %mM Association constant
vdeg = 2*300*10^(-6)/60; %mM/s

%Pfk formation rate calculated in Appendix H
pfk_form = 5.76*10^(-7); %mM/s

%Degradation term
deg= vdeg*(sspB/(Kas+sspB)*y(3))/(Km+y(3));

%ODE sets that describes the experimental system
dpfkdt=pfk_form-mu*y(3)-deg;
df6pdt=rpgi-rpfk-deg-mu*y(2);
dg6pdt=rpts-rpgi-mu*y(1);

dy = [dg6pdt;df6pdt;dpfkdt];

end


function ss=max1(c,k,vmax,mu)
%Parameters from Chassagnole et al.
Lpfk = 5629067;
npfk = 11.1;
npts = 3.66;

%Rate of reactions
```

```
rpts =
vmax(1)*c(1)*c(2)/c(3)/((k(1)+k(2)*c(2)/c(3)+k(3)*c(1)+c(1)*c(2)/c(3))*(1+(c(
8))^npts/k(4)));

rpgi = vmax(2)*(c(8)-
c(9)/k(17))/(k(5)*(1+c(9)/(k(6)*(1+c(5)/k(7)))+c(5)/k(8))+c(8));

A = 1+c(2)/k(12)+c(6)/k(13)+c(7)/k(14);
B = 1+c(6)/k(15)+c(7)/k(16);

rpfk =
vmax(3)*c(4)*c(9)/((c(4)+k(9)*(1+c(6)/k(10)))*(c(9)+k(11)*A/B)*(1+Lpfk/((1+c(
9)*B/((k(11))^A))^npfk)));
pfk_form = 5.76*10^(-7); %mM/s

rzwf =
vmax(4)*c(8)*c(11)/((c(8)+k(18))*(1+c(12)/k(19))*(k(20)*(1+c(12)/k(21))+c(11)
));

%ODE set used to calculate maximum velocities in the rate of reactions
dg6pdt=rpts-rpgi-mu*c(8)-rzwf;
df6pdt=rpgi-rpfk-mu*c(9)+0.5*rzwf;
dpfkdt=pfk_form-mu*c(10);
dpgidt =rpgi-4*rzwf; %follow flux distribution reported by Zhao et al.

ss = [dg6pdt;df6pdt;dpfkdt;dpgidt];

end

function [du] = Cph8Ompr_ODEs(Ir,t,u,kp,kg)

du = zeros(2,1);

%ODE set that describes the Cph8-OmpR system
du(1) = kp*(c_Cph8Ompr(Ir, t) - u(1));
du(2) = kg*(u(1)-u(2));

end

function [c] = c_Cph8Ompr(Ir, t)
```

```
b = 12.5;
a = 85.9;
n = 1.39;
k = 0.0243;

c = b+a*(k^n / (Ir(t)^n + k^n));
end

end
```

APPENDIX L

Appendix L contains supporting gel images.

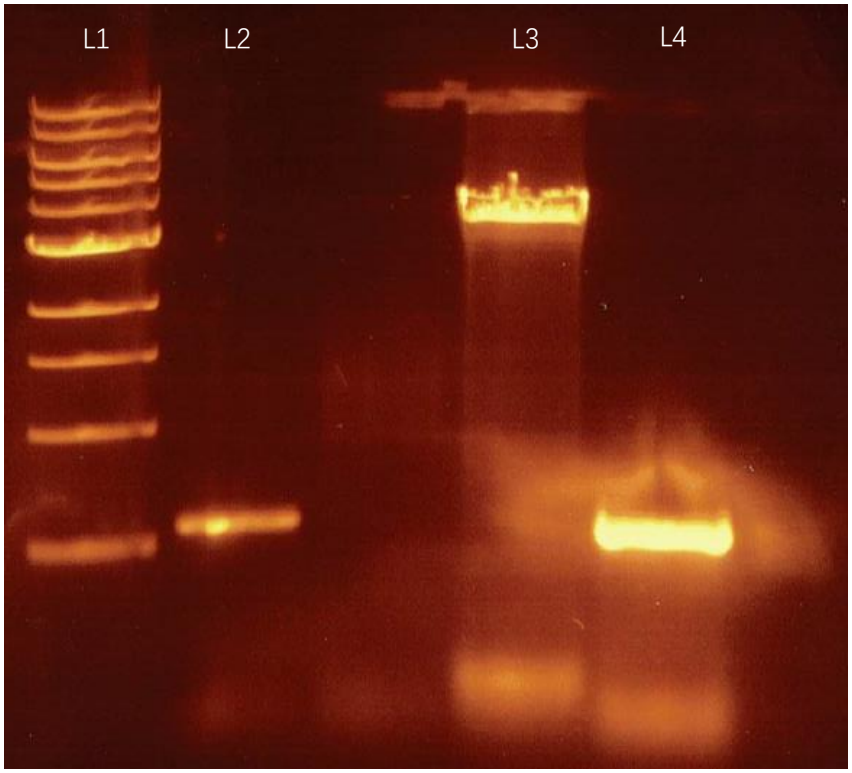

Figure L1 Gel image of successful backbone and insert amplification. Lane 1: 1kb ladder; Lane 2/4: SspB fragment (717 bp); Lane 3: pSR59.4 backbone without sfGFP (4646 bp).

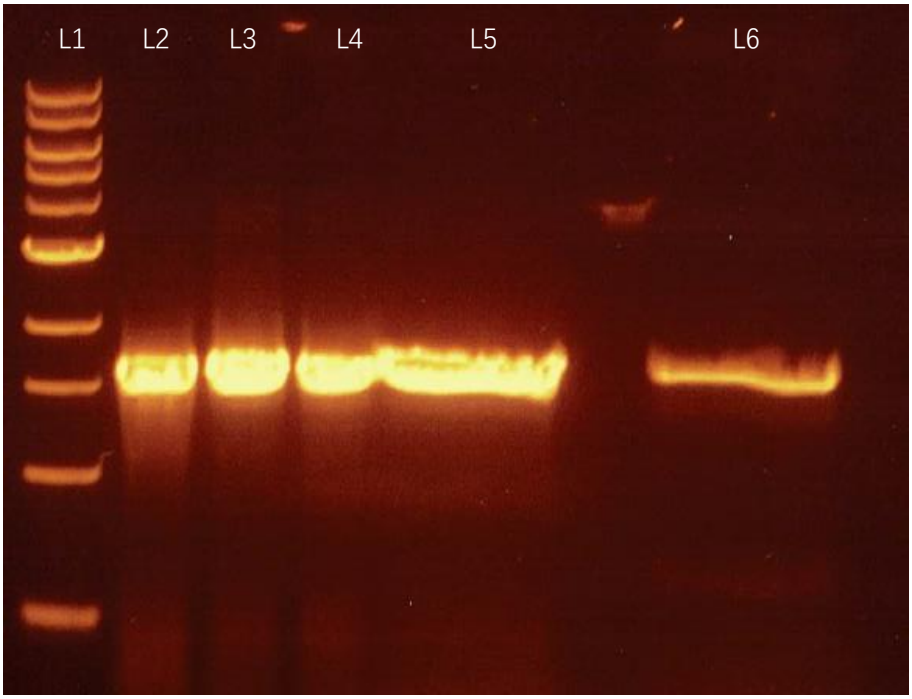

Figure L2 Gel image of successful kanamycin cassette amplification. Lane 1: 1kb ladder; Lane 2/3/4: PCR product with OneTaq; Lane 5/6: PCR product with Q5 polymerase.

APPENDIX M

Calculate the change in G6P production amount according to Figure 15.
Take the difference between the end points from the two light intensities:

$$\Delta = 5.6817 * 10^{-5}\ mM = 5.6817 * 10^{-8}\frac{mol}{L}$$

Volume of an *E. coli* cell:

$$\mathrm{V}_{cell} = 5.236 * 10^{-16}\frac{L}{cell}$$

At OD600 equals 1.0, number of cells present in the culture is approximately:

$$\mathrm{N} = 8 * 10^{8}\frac{\mathrm{cell}}{mL}$$

A normal pilot reactor is 1L: $\mathrm{V}_r = 1\ L = 1000\ mL$

Molecular weight of G6P: $\mathrm{MW} = 260.136\ \mathrm{g/mol}$

$$\Delta_{total} = \Delta * V_{cell} * N * V_r * MW$$

$$\Delta_{total} = 5.6817 * 10^{-8}\frac{mol}{L} * 5.236 * 10^{-16}\frac{L}{cell} * 8 * 10^{8}\frac{cell}{mL} * 1000\ mL * 260.136\frac{g}{mol}$$

$$\Delta_{total} = 6.19 * 10^{-9}\ g = 6.19\ \mathrm{ng}$$

APPENDIX N

Table N1 Major assumptions used in the mathematical modeling

In wild type *E. coli* to estimate maximum velocities		
Result	Assumptions	References
$r_{PGM} = 0$	Negligible consumption according to flux distribution diagram	[10]
$r_{MurSynth} = 0$	Negligible consumption according to flux distribution diagram	[10]
$r_{TKb} + r_{TA} = 0.5 r_{G6PDH}$	Return of F6P from PPP is half of that entering PPP	[5]
$r_{PGI} = 4 r_{G6PDH}$	The amount of carbon flux processed by Pgi from G6P to F6P is four times of that processed by PPP	[19]
In experimental system where G6PDH was deleted		
Result	Assumptions	References
$r_{G6PDH} = 0$	G6PDH gene was knocked out	[5]
$P_{pfk} = P_{pfk-I}$	All Pfk produced is assumed in its major form Pfk-I	[5]
$v_{pfk,max} = v_{pfk,max,0} \frac{[pfk]}{[pfk]_0}$	Maximum velocity of Pfk-I in the experimental system changes linearly with respect to varying Pfk concentration	N/A
$\text{degradation} = \frac{V_{max}[pfk]}{K_{m,app} + [pfk]}$	Assume the degradation term follows a Michaelis-Menten kinetics: 1) The concentration of complexes approaches steady-state rapidly; 2) The sum of free enzyme and enzyme complex is the total amount of enzyme; 3) Product formation is the rate-limiting step	N/A
$V_{max} = v_{max,app}\left(\frac{[sspB]}{K_{m,sspB} + [sspB]}\right)$	Assume the maximum velocity of degradation is a function of SspB and it follows Michaelis-Menten kinetics	N/A

APPENDIX O

Appendix O shows the desired strain with correct plasmids. The left plasmid would be the new construct, while the right one would be adopted from Cph8-OmpR system. The genome would be modified with both *envZ* gene and *sspB* gene knocked out.

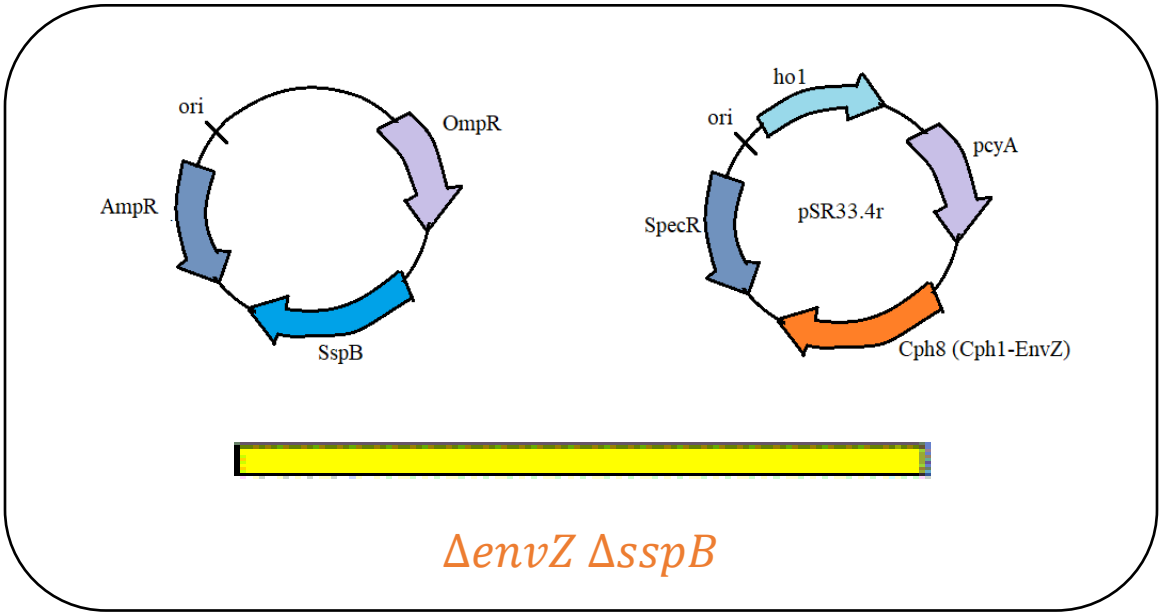

APPENDIX P

Degradation model from mathematical deduction:

$E_1 + S \rightleftharpoons X_1$ forward reaction constant: k_1 backward reaction constant: k_{-1}

$X_1 + E_2 \rightleftharpoons X_2$ forward reaction constant: k_2 backward reaction constant: k_{-2}

$X_2 \rightarrow E_2 + E_1 + P$ forward reaction constant: k_3 No backward reaction

$$\frac{d[E_1]}{dt} = -k_1 E_1 S + k_{-1} X_1 + k_3 X_2$$
$$\frac{d[E_2]}{dt} = -k_2 E_2 X_1 + k_{-2} X_2 + k_3 X_2$$
$$\frac{d[S]}{dt} = -k_1 E_1 S + k_{-1} X_1$$
$$\frac{d[X_1]}{dt} = k_1 E_1 S - k_{-1} X_1 - k_2 X_1 E_2 + k_{-2} X_2$$
$$\frac{d[X_2]}{dt} = k_2 X_1 E_2 - k_{-2} X_2 - k_3 X_2$$
$$\frac{d[P]}{dt} = k_3 X_2$$

Assumptions:
No backward reaction during product (degraded material) formation step
The enzyme-substrate complexes X_2 and X_1 concentrations are nearly at steady-state
$E_1 + X_1 + X_2 = E_{T1}$ $E_2 + X_2 = E_{T2}$ where E_{T1} and E_{T2} are the total enzyme concentrations

$$k_1 E_1 S - k_{-1} X_1 - k_2 X_1 E_2 + k_{-2} X_2 = 0$$
$$k_2 X_1 E_2 - k_{-2} X_2 - k_3 X_2 = 0$$

Substitute $E_1 = E_{T1} - X_2 - X_1$ into the first equation and solve for X_1

$$X_1 = \frac{k_1 X_2 S - k_1 E_{T1} S - k_{-2} X_2}{k_2 X_2 - k_2 E_{T2} - k_{-1} - k_1 S}$$

Then substitute $E_2 = E_{T2} - X_2$ and X_1 expression obtained above into the second equation

$$k_2 (E_{T2} - X_2) \frac{k_1 X_2 S - k_1 E_{T1} S - k_{-2} X_2}{k_2 X_2 - k_2 E_{T2} - k_{-1} - k_1 S} - (k_{-2} + k_3) X_2 = 0$$

Solve for X_2

$$a X_2^2 + b X_2 + c = 0$$

$$\mathrm{a} = -k_1 k_2 S - k_3 k_2$$

$$\mathrm{b} = \mathrm{k}_1 k_2 E_{T2} S + \mathrm{k}_1 k_2 E_{T1} S + k_3 k_2 E_{T2} + (k_{-2} + k_3) k_{-1} + (k_{-2} + k_3) k_1 S$$

$$\mathrm{c} = \mathrm{k}_1 k_2 E_{T1} E_{T2} S$$

$$\mathrm{X}_2 = \frac{-b \pm \sqrt{b^2 - 4ac}}{2a}$$

Since all the reaction constants and protein concentrations are positive, the following will always be true:

$$\mathrm{a} < 0$$
$$\mathrm{b} > 0$$
$$\mathrm{c} > 0$$

Therefore

$$\sqrt{\mathrm{b}^2 - 4ac} > \mathrm{b} > 0$$

$$-\mathrm{b} + \sqrt{\mathrm{b}^2 - 4ac} > 0 \qquad -\mathrm{b} - \sqrt{\mathrm{b}^2 - 4ac} < 0$$

$$\mathrm{X}_2 = \frac{-b+\sqrt{b^2-4ac}}{2a} < 0 \qquad \mathrm{X}_2 = \frac{-b-\sqrt{b^2-4ac}}{2a} > 0$$

The first root becomes biologically irrelevant.

$$\text{degradation} = \; k_3 X_2 = k_3 \frac{-b - \sqrt{b^2 - 4ac}}{2a}$$